DRAFT

Shrinkage and Thermal Cracking of Fast Setting Hydraulic Cement Concrete Pavements in Palmdale, California

Preliminary Report Prepared for

CALIFORNIA DEPARTMENT OF TRANSPORTATION

By

Andrew C. Heath and Jeffery R. Roesler

December 1999

Executive summary

Jointed Plain Concrete Pavement (JPCP) test sections were constructed using Fast Setting Hydraulic Cement Concrete (FSHCC) as part of the California accelerated pavement testing program (CAL/APT). Many of the longer slabs cracked under environmental influences before any traffic load was applied to them. Cores drilled through the cracks indicated that cracking initiated at the top of the slabs and propagated downwards. Concrete shrinkage and thermal strain data from field instrumentation was recorded and analyzed along with laboratory test data to determine the cause of the cracking. Finite element analysis using the measured strains and temperatures predicted high tensile stresses at the top of the test section slabs as a result of the differential drying shrinkage between the top and base of the slab and the non-linear nature of the negative temperature gradients through the slab. Laboratory free shrinkage tests on the test section cement indicated significantly higher shrinkage than ordinary Type II Portland cement.

Based on the analysis it is recommended that the use of high shrinkage hydraulic cements in rigid pavement construction should be discouraged as these can result in high differential shrinkage gradients and premature cracking. Laboratory tests indicated fast setting hydraulic cements do not necessarily have high shrinkage and some can have significantly lower shrinkage than typical Type II cements. Shorter slab lengths (<4.5 m) will reduce tensile stresses and thereby reduce the chance of premature failure in the event high shrinkage cement is used. Stiff bases such as lean concrete bases, will increase the stresses in pavements because of friction between the base and slab. Bases which are flexible under long-term loading and stiff under short-term traffic loading (for example asphalt concrete bases) are preferred.

TABLE OF CONTENTS

TABLES

FIGURES

1 INTRODUCTION

In order to minimize lane closures, Caltrans proposed the use of Fast Setting Hydraulic Cement Concrete (FSHCC) for the reconstruction of some urban freeways. Caltrans has been using FSHCC to do full-depth concrete repair on night-time closures to more consistently achieve concrete flexural strengths high enough for opening to truck traffic within hours after casting of the concrete.

No controlled research has been conducted on the structural performance of FSHCC under repeated loading. Caltrans has designed and constructed test sections using FSHCC along State Route 14 near Palmdale, California to determine the fatigue resistance of FSHCC.

Shortly after construction, many of the slabs in the test sections cracked under environmental loading before any traffic loading was applied. The environmental loading resulted in transverse cracking through the middle of the slab, as illustrated in Figure 1.1. This report is an investigation into the failure of these FSHCC slabs through field measurements, laboratory testing and finite element analysis.

Figure 1.1. Transverse environmental cracking through the center of a slab

2 LITERATURE

Although there has been a great deal of research conducted on the effects of shrinkage and thermal gradients on concrete pavement performance, there is no generally accepted procedure for analyzing this problem. Most current analyses concentrate on stresses from thermal gradients (Khazanovich, 1994 and Hansen, 1997), while the modeling of the concrete drying shrinkage and thermal contraction, the interface between the slab and the base, the variation in moisture conditions in the slab, and the interaction with other slabs is less understood and accounted for.

2.1 Thermal stress analysis

The concrete strain due to changes in temperature follows the following form within the range of typical pavement temperatures:

$$e_t = a \cdot \Delta T$$

Where : ε_t is the thermal strain

α is the concrete coefficient of thermal expansion

ΔT is the change in temperature

The coefficient of thermal expansion for concrete is influenced more by aggregate type than by any other factor (Tia et al, 1991). Quartz has the highest coefficient of thermal expansion of the common minerals and the coefficient of thermal expansion of concrete is often related to the quartz content of the aggregates.

2.1.1 Bending stresses

Upward or downward curling of the slab induce bending stresses in the concrete. Upward temperature curling typically occurs at night when the top of the slab contracts relative to the bottom of the slab and downward temperature curling typically occurs during the day when the top of the slab expands relative to the bottom of the slab. These two cases are illustrated in Figure 2.1.

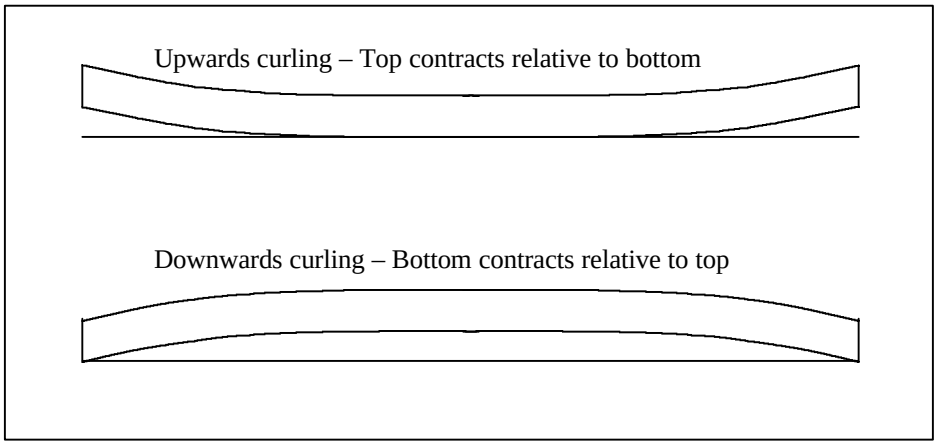

Figure 2.1. Upwards and downwards curling geometry

2.1.1.1 Linear temperature distribution

Some of the first concrete pavement thermal stress analyses were performed in the 1920's (Westergaard, 1927). The Westergaard analyses use plate theory to determine the deflections, strains and stresses at the center, edge and corner of a semi-infinite concrete slab subjected to a linear temperature distribution with depth. Bradbury later enhanced Westergaards's models to account for varying pavement geometry and slab stiffness (Bradbury, 1938). The general form of the equation to determine the maximum stress in

a concrete pavement subjected to a linear temperature distribution is as follows:

$$s = \frac{E \cdot a \cdot \Delta T}{2(1-u^2)} \cdot (Cx + u \cdot Cy)$$

Where : σ is the maximum stress at the top or base of the slab

E is the Young's modulus of the concrete

α is the coefficient of thermal expansion

ΔT is the difference in temperature between the top and base of the slab

ν is the Poisson's ratio of the concrete

Cx and Cy are correction factors related L/ℓ, where L is the slab length and ℓ is the radius of relative stiffness:

$$\ell = \sqrt[4]{\frac{E \cdot h^3}{12(1-u^2)k}}$$

Where : h is the thickness of the slab

k is the modulus of subgrade reaction

As the ratio of L/ℓ increases, higher curling stresses will result. This ratio will increase for longer slabs, thinner slabs, lower modulus concrete, and stiffer subgrades.

2.1.1.2 Non-linear temperature distribution

Although the Westergaard and Bradbury analyses are still widely used today, a number of researchers have identified the need for improved pavement analyses which take the non-linear nature of temperature gradients into account (Khazanovich, 1994 and Hansen, 1997).

The development of the ILSL2 computer program at the University of Illinois enabled the stresses from general non-linear temperature distributions to be determined using the finite element method (Khazanovich, 1994). As illustrated in Figure 2.2, ILSL2 fits a curve function to the difference in temperatures between a calculated linear temperature distribution and the actual non-linear distribution. This curve function is selected so that the sum of the moments is equal to zero, therefore all stresses from the curve are axial in nature and simple to determine. ILSL2 then determines the linear temperature gradient through the slab by subtracting the axial curve distribution from the actual non-linear distribution. The linear gradient is used to calculate the curling stresses in the slab using the finite element method. Since linear elasticity is assumed for the concrete slab, the axial only stresses from the parabolic temperature distribution can then added to the curling stresses from the linear distribution. Addition of the linear stresses and axial stresses will give the same stresses as the nonlinear temperature distribution.

Researchers at the University of Michigan later proposed a similar method of analysis where a parabolic curve function is fitted to the temperature data (Mohamed and Hansen, 1997). A limitation of the Mohamed and Hansen method is that only parabolic functions can be fitted to the data while the actual temperature distributions are not necessarily parabolic in nature. As shown later in this report, the most critical temperature loading situation for this project was when the surface of the slab was rapidly cooled on a hot day (for example by a rainstorm). A parabolic temperature distribution does not effectively capture this situation and can result in predicted stresses lower than actual stresses.

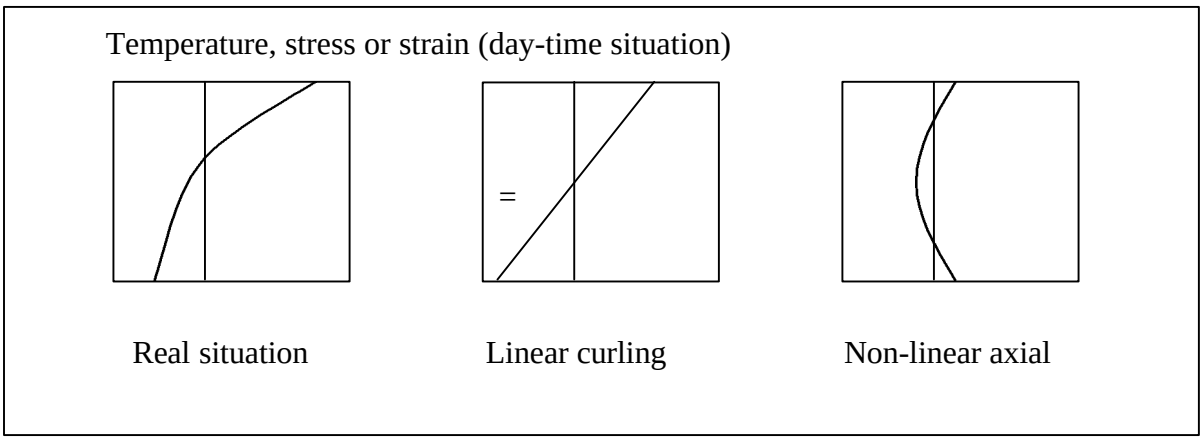

Figure 2.2. Converting non-linear temperature distribution to axial and equivalent linear distribution.

When comparing linear to non-linear temperature gradients, stresses calculated using typical non-linear pavement temperature gradients have the following effect on compressive and tensile stresses in slabs:

Table 2.1. Effect of using non-linear instead of linear temperature distribution.

Temperature distribution	Max compressive stress	Max tensile stress
Positive (day time)	Top of slab Higher for non-linear	Base of slab Lower for non-linear
Negative (night time)	Base of slab Lower for non-linear	Top of slab Higher for non-linear

As concrete is approximately one order of magnitude weaker in tension than in compression, the increase in tensile stress during a typical night time temperature gradient is the most important condition to investigate.

2.1.2 Axial stresses

Although a good deal of work investigating the frictional bond between bases and slabs has been performed, this is often ignored in analyses. Most current analyses still assume either a fully bonded or fully unbonded slab/base interface in the vertical direction but ignore the horizontal friction factor. The horizontal friction between the base and slab can have a significant effect on the concrete tensile stresses. The classical frictional resistance model has the following form:

$$t = m \cdot N$$

Where: τ is the frictional force

μ is the coefficient of friction along the sliding plane

N is the normal force applied to the sliding plane

Previous research (Wimsatt et al, 1987, Wesevich et al, 1987) has shown that determining the friction between a concrete slab and a base is not a trivial analysis, as the friction does not follow the classical model. It is instead made up of a number of components, namely adhesion, shear and bearing, as illustrated in Figure 2.3

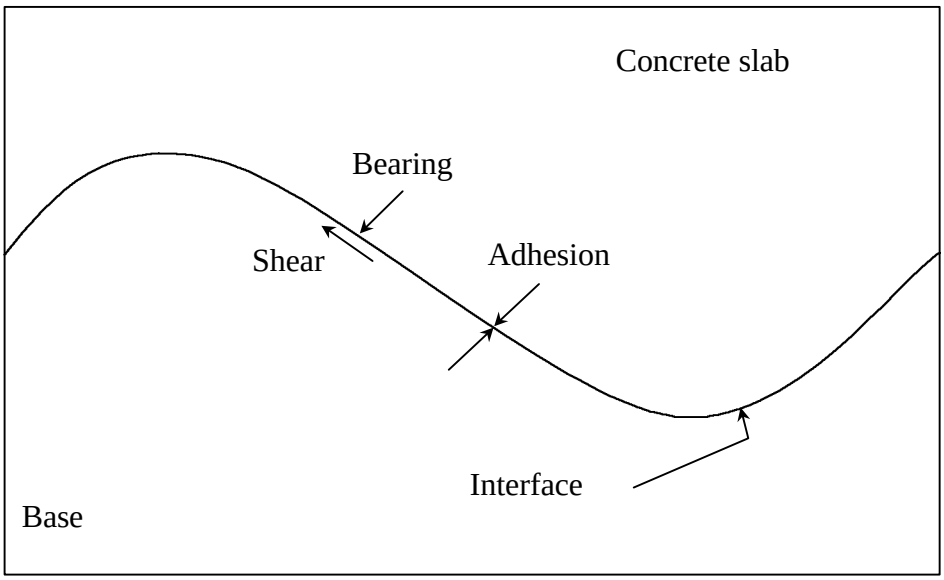

Figure 2.3. Components of slab/base friction.

The friction between the slab and base depends on the base type and the differential movement between the slab and the base and is not proportional to the normal force, as is the case with the classical friction model. The general form of the frictional stress verses displacement relationship can be approximated by assuming a parabolic function for small displacements and an asymptotic limit for some level of displacement after which the frictional stress remains constant. Typical values for the stresses induced in different base types are given in Figure 2.4 (Wimsatt et al, 1987, Wesevich et al, 1987). The frictional stress is a shear stress given for a square meter of pavement/base interface and is largely independent of slab thickness and bearing stress. Under field conditions, the frictional stress can often increase or decrease slightly after the steady state condition is achieved, but this is difficult to quantify.

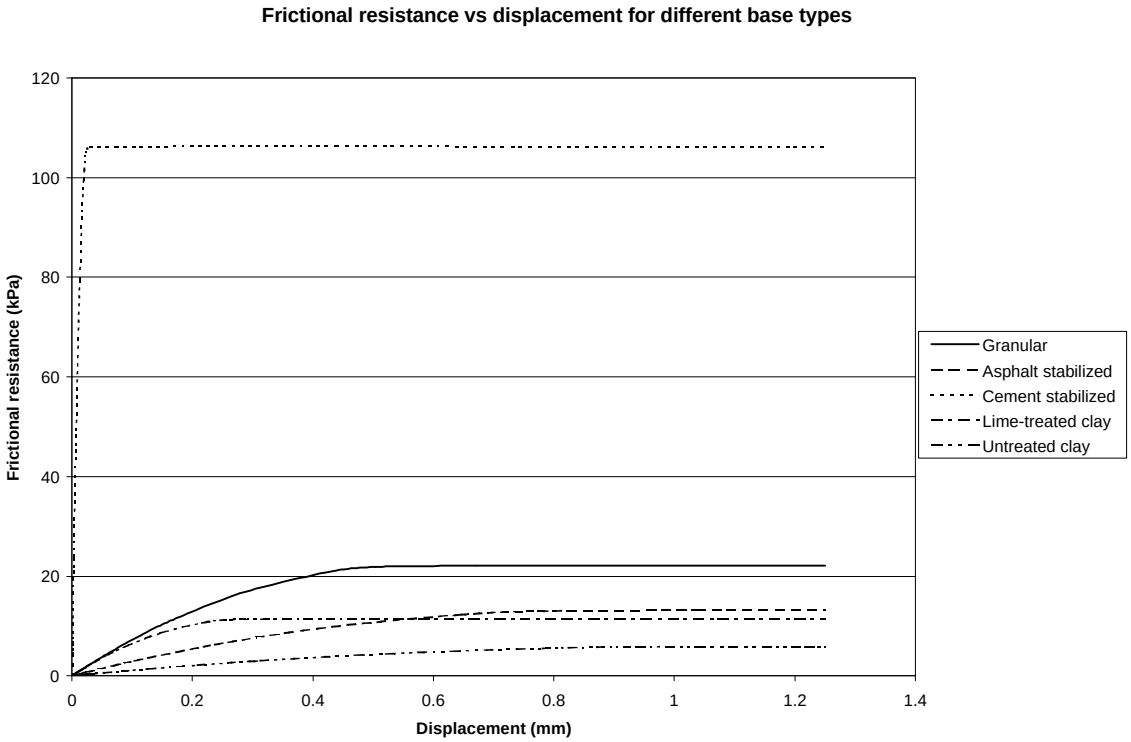

Figure 2.4. Typical frictional resistance, displacement relationships.

As shown in Figure 2.4 the frictional stress between a slab and a cement stabilized base is higher than for any other base type. The cement stabilized base also requires the least movement to mobilize the maximum friction force, probably because of the high stiffness of this layer.

Researchers also investigated different friction reducing layers between concrete slabs and cement treated bases (PCA, 1971). It was found that a 6 mm sand layer with polyethylene sheeting above it, or a double polyethylene layer were the most effective methods of reducing friction between a slab and cement treated base. With these types of friction reducing layers, a more classical friction model can be used where the friction force is proportional to normal force on the friction plane. Placing sand under a slab

could, however, lead to excessive erosion and faulting.

In the case of the two above mentioned friction reducing layers, the coefficient of friction, μ, varied between approximately 0.50 and 0.80. The tensile stresses from uniform contraction of a slab can be determined for the case where the slab is in uniform contact with the base and the full frictional resistance is mobilized. If the slab was 200 mm thick and 4.5 m long, with a coefficient of friction of 0.65 between the slab and base, a frictional stress of approximately 35 kPa per square meter of slab / base interface will result. This is significantly less than the stress for a base without a friction reducing layer (Figure 2.4). The maximum tensile stress in the concrete slab with a friction reducing layer would be approximately 175 kPa while it would be closer to 1180 kPa (1.2 MPa) for the same slab on a cement stabilized base. The maximum stress would occur in the center of the slab for both cases. If full contact between the slab and base was not achieved (for example if the upwards curling occurred), the frictional stress would be reduced.

In addition to the axial stresses from daily temperature variations, tensile stresses will develop when the concrete slab cools from the high heat of hydration during construction to lower ambient temperatures. The tensile stresses will be highest when setting occurs during the heat of the day during the summer months since the slab would have a higher temperature to cool from.

If a new concrete slab bonds to an existing adjacent slab edge (load transfer devices or concrete surface), the contraction of the new concrete will create high tensile stresses in the new slab because of the restraint from the existing slab.

2.2 Shrinkage stress

Drying shrinkage occurs in concrete as a result of moisture loss within the cement paste. A portion of this drying shrinkage will be elastic (recoverable) and a portion plastic (unrecoverable). This shrinkage can cause both bending and axial stresses in concrete slabs. The drying shrinkage of concrete slabs will vary, depending on the concrete mix components and curing and environmental conditions.

The shrinkage of concrete will be higher for the unrestrained case (free shrinkage) than for the partially restrained case (shrinkage restricted). The partially restrained case is further complicated by elastic deformations and creep, brought about by boundary conditions acting on the concrete specimen (Farrington, et al, 1996). The creep of concrete will reduce the stresses due to shrinkage of concrete pavement slabs.

Different models exist where the rate of concrete shrinkage can be calculated as a function of the moisture conditions, the cement shrinkage, the quantity of aggregate and the elastic properties of the concrete (Ruth, 1993). The major problem with this approach is the relationship is for calculating unrestrained concrete shrinkage, which is not the true field situation. Another problem is a large number of parameters are required, of which the relative humidity at different depths in the pavement is difficult to determine.

2.2.1 Bending stress

The drying shrinkage of a concrete slab is non-uniform because of the different moisture and evaporation conditions at the surface and base of the slab. This shrinkage gradient can have the same curling effect as the night time temperature situation where the top of the slab contracts more than the bottom of the slab, as illustrated in Figure 2.1.

This is because the top of the slab looses moisture as it is exposed to the environment (sunlight, air, and wind) and therefore shrinks more than the bottom of the slab.

A model proposed by Rasmussen and McCullough assumes that the full shrinkage occurs at the surface of a concrete pavement and no shrinkage occurs below the mid-depth of the slab (Rasmussen and McCullough, 1998). The shrinkage is assumed to decrease in a linear manner between the top and center of the slab, as shown in Figure 2.5.

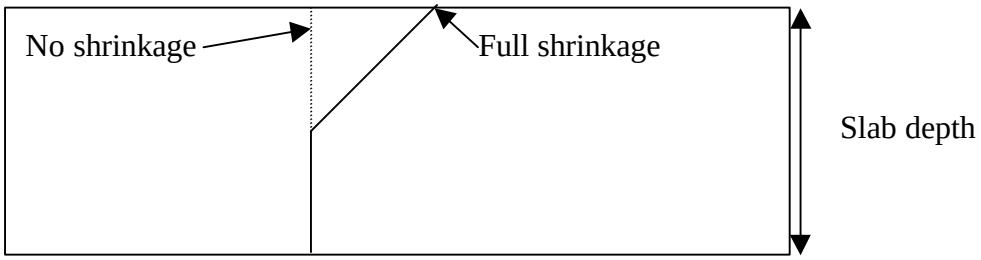

Figure 2.5. Slab shrinkage gradient assumed by Rasmussen and McCullough (1998)

The stresses from differential shrinkage can be modeled by calculating an equivalent temperature distribution for the slab, which can then be used to determine the curling stresses.

2.2.2 Axial stress

The stresses caused by axial shrinkage and base friction can be modeled in the same manner as stresses from axial thermal contraction.

2.3 Relationship between stress and concrete strength

2.3.1 Combined thermal and shrinkage stresses

Since the temperature at the top of a concrete slab varies more than that at the base, the neutral axis of bending will typically be closer to the top of the slab. During the typical night time situation, the non-linear axial and linear curling components of the temperature distribution add to each other at the top of the slab resulting in high tensile stresses.

Because of concrete shrinkage, the friction between a pavement slab and the base will always result in tensile stresses in the slab. As the top of the slab shrinks more than the bottom, upwards curling similar to nigh time temperature curling will occur, resulting in tensile stresses near the surface of the slab.

Frictional stresses caused by the concrete slab cooling from the heat of hydration will be tensile. These stresses will be highest when the slab is at its coolest (during the night) and when paving was performed during the heat of the day.

As the strain magnitudes in concrete slabs are generally low, linear elasticity is assumed and the tensile stresses from temperature changes can therefore be added to those from shrinkage, taking the orientations of the stresses into account.

2.3.2 Concrete strengths

Portland Cement Concrete (PCC) strengths usually increase with time as a result of the curing process. Increased moisture promotes better curing, as water is needed for

the hydration of the cement. Other rapid setting hydraulic cements have a different chemistry, which can result in little strength increase after the initial strength gain.

For PCC, the strength increase follows a roughly log-linear increase with time. However, if the concrete has little or no access to water, the strengths will be significantly less than for the moist cured condition. Although curing membranes are often placed over concrete slabs immediately after construction, evaporation from the concrete still occurs (McCullough and Dossey, 1999). Double curing membranes are more effective than single curing membranes.

The loss of moisture near the surface of a slab can lead to the concrete tensile strength being up to 2.75 MPa less than that at the base of the slab in areas where there is high evaporation (McCullough and Dossey, 1999). This reduction in strength near the surface can be over 50 percent of the moist cured tensile strength.

2.3.3 Combined critical stresses

The highest environmental stresses can be at the surface of the slab which is also the location of the lowest concrete strength. Environmentally induced cracks are therefore likely to initiate at the surface of the slab. Cores drilled through cracks in the Palmdale test sections revealed that the cracks do initiate at the surface, as some surface cracks had not propagated to the bottom of the slab, as shown in Figure 2.6.

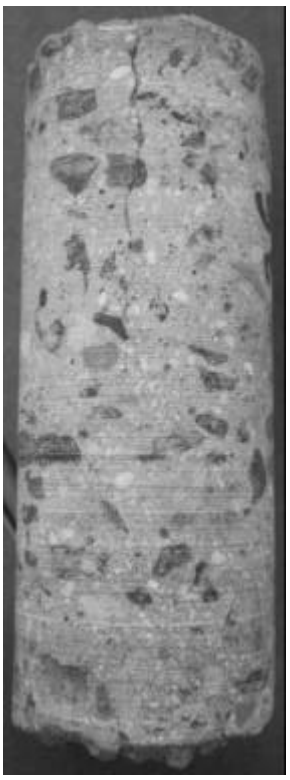

Figure 2.6. Core showing crack initiation at the surface of the slab.

3 FIELD DATA

3.1 Overview

3.1.1 Test section layout

Six test sections were constructed, three to determine the effect of different slab thickness on pavement performance, and three to investigate the effects of different shoulder types and dowel placement on pavement performance. The layout of the test sections is shown in Figure 3.1.

Figure 3.1. Layout of test sections.

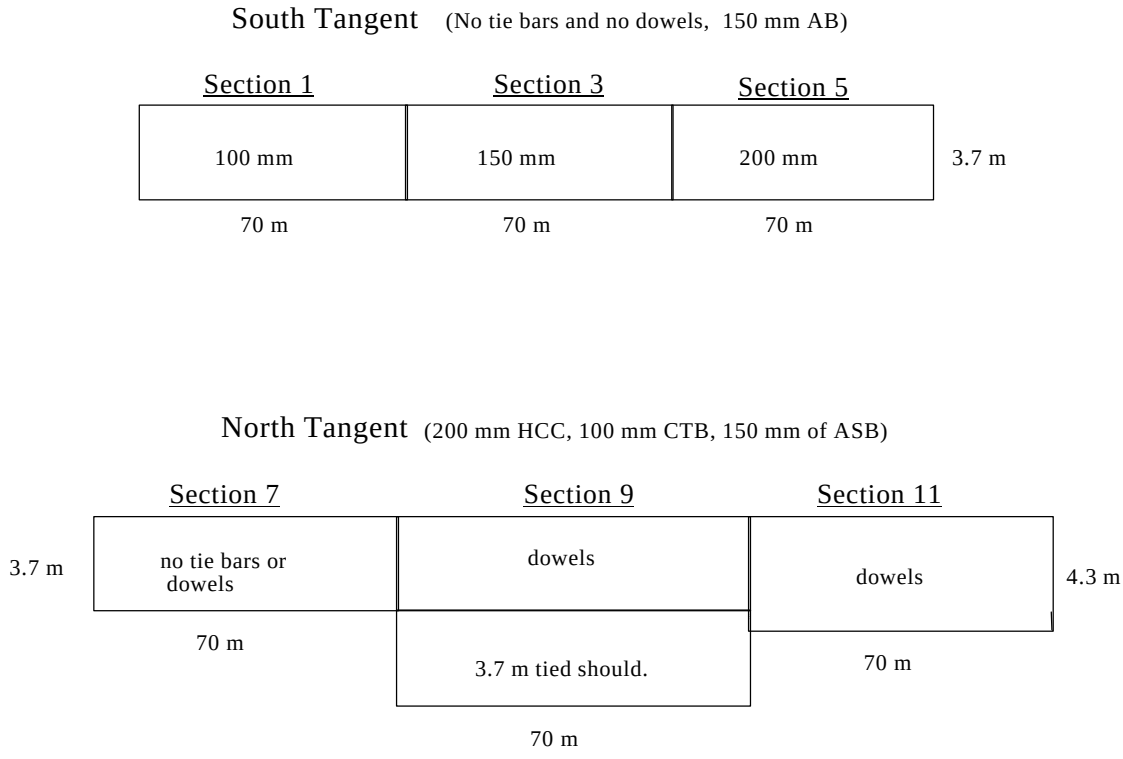

The north and south tangents are on the northbound and southbound lanes of SR 14 respectively. Each section has approximately 15 slabs.

3.1.2 Instrumentation

The test sections had a variety of instrumentation and data acquisition systems installed. The relevant instrumentation is described in detail in the following sections. The location of some of the instrumentation is illustrated in Appendix A. The data acquisition systems were either continuously monitored, taking readings every two hours, or were connected to the instrumentation only when needed.

3.1.3 Field performance

The test sections were constructed in June 1998. It was intended that the data acquisition units would record data immediately prior to construction so that strains, temperatures and displacements in the slabs immediately after construction could be determined.

Within two months of construction, cracking was observed in the slabs that had only been subjected to the environment. Within three months after construction, almost all of the longer slabs (5.5 and 5.8 m long) had cracked under environmental influences. The location of the cracks are shown in detail in Appendix A. The slab thickness and load transfer mechanisms for the different test sections are given in Figure 3.1. Most of the environmental cracks were transverse cracks through the center of the slab.

The environmental cracking would have occurred when the tensile stresses in the slab as a result of the thermal strains and shrinkage would have exceeded the tensile strength of the concrete.

3.2 Concrete properties

3.2.1 Mix design

The fast setting concrete mix used in the construction of the test sections was designed by the contractor and approved by Caltrans after the contractor paved a test section. Details of the mix design can be found in Roesler et al, 1999. The contractor used a cement blend of 80 % calcium sulfo-aluminate (CS̄A) and 20% Type II cement for this project.

Descriptions of the materials and the mix design used in the construction of the test sections are given in Table 3.1.

Table 3.1. Materials description and mix design used in the construction of test sections.

Material	Description	% mass dry agg	kg/m^3 concrete
Coarse aggregate	26 mm maximum size, Gabbro material, Relative density = 2.83, Water absorption = 1.30%.	56.8	1116
Fine aggregate	4.75 mm maximum size, Mainly quartz material, Relative density = 2.68, Water absorption = 1.43%.	43.2	849
CS̄A Cement	Fast setting hydraulic cement, Calcium sulfoaluminate type cement.	17.7	348
Type II Portland Cement	Typical type II Portland cement, supplied by the contractor.	4.4	86
Delvo® Admixture	Chemical retarder to increase set time.	0.26	4.2
Micro-Air® Admixture	Chemical air entraining agent.	0.0037	59 g/m^3
Water / Cement Ratio	Target for the construction – average was closer to 0.44.	0.39	0.39

3.2.2 Field strength testing

The strength of the concrete mix was tested using compressive and flexural strength tests. The flexural testing was performed as either third point or center point beam testing. Only the average compressive strength and average third point beam testing are given in Table 3.2. The additional results are available in the report on the construction of the test sections (Roesler, et al. 1998).

Table 3.2. Average concrete compressive and flexural strength.

Time after placing	Ave compressive strength (F'_C)		Ave flexural strength (M_R)	
	Strength (MPa)	Std deviation (MPa)	Strength (MPa)	Std deviation (MPa)
8 Hours	13.57	2.65	2.09	0.32
7 Days	28.68	5.15	4.03	0.54
90 Days	45.50	7.74	5.14	0.79

The average compressive and flexural strengths are illustrated in Figure 3.2.

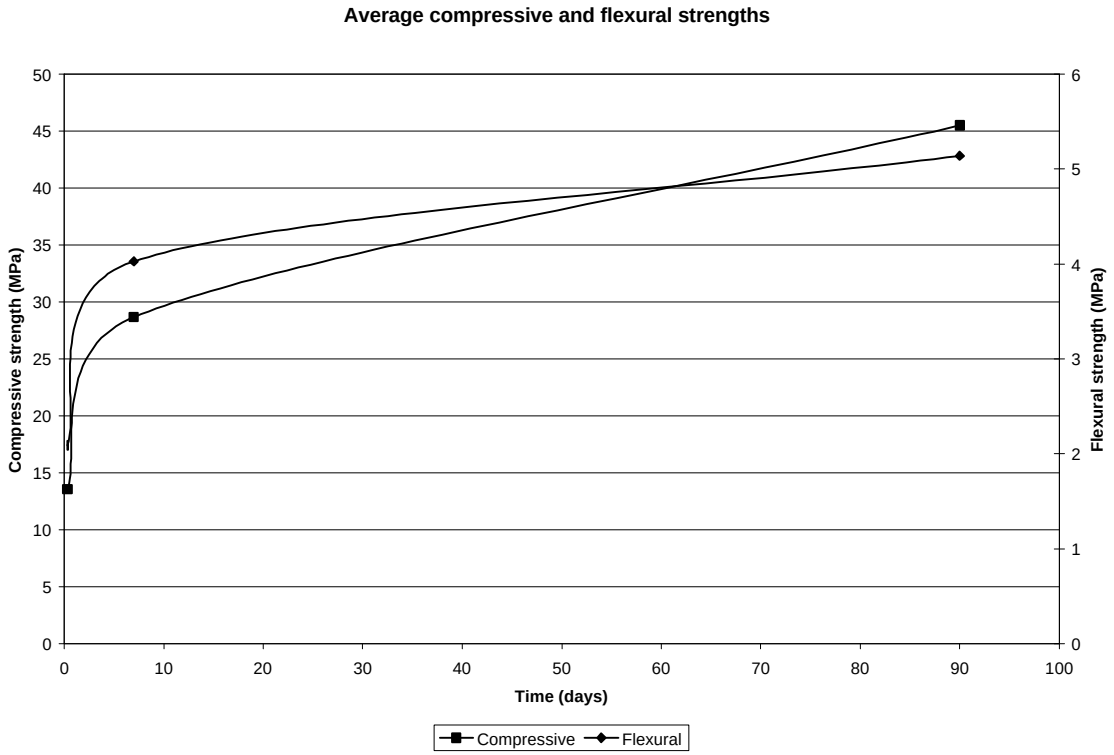

Figure 3.2. Average concrete compressive and flexural strengths.

3.3 Climate

Climatic data at the test section site was obtained from an on site weather station, which recorded the pertinent data such as the maximum and minimum temperatures, humidity, rainfall and wind-speed. Data was recorded every two hours by an automatic data acquisition unit.

A summary of the temperature, rainfall and humidity data from just after construction of the test sections (July 1998) until the end of March 1999 is given in Table 3.3, while the temperature data is summarized in Figure 3.3 below.

Table 3.3. Average monthly temperatures, total rainfall and average humidity.

Month	Ave daily max temp (ºC)	Ave daily min temp (ºC)	Ave temp (ºC)	Total rainfall (mm)	Ave relative humidity (%)
July-98	33.9	22.6	26.9	0.6	34.9
August-98	34.8	22.7	27.2	5.2	32.5
September-98	27.0	16.0	19.8	10.0	55.4
October-98	22.0	12.3	15.8	1.6	37.8
November-98	17.0	8.2	11.2	16.2	46.7
December-98	12.0	4.3	7.2	9.2	38.8
January-99	14.7	6.7	9.3	18.2	43.6
February-99	14.4	5.5	8.8	4.8	48.3
March-99	16.1	5.9	9.4	9.6	55.6

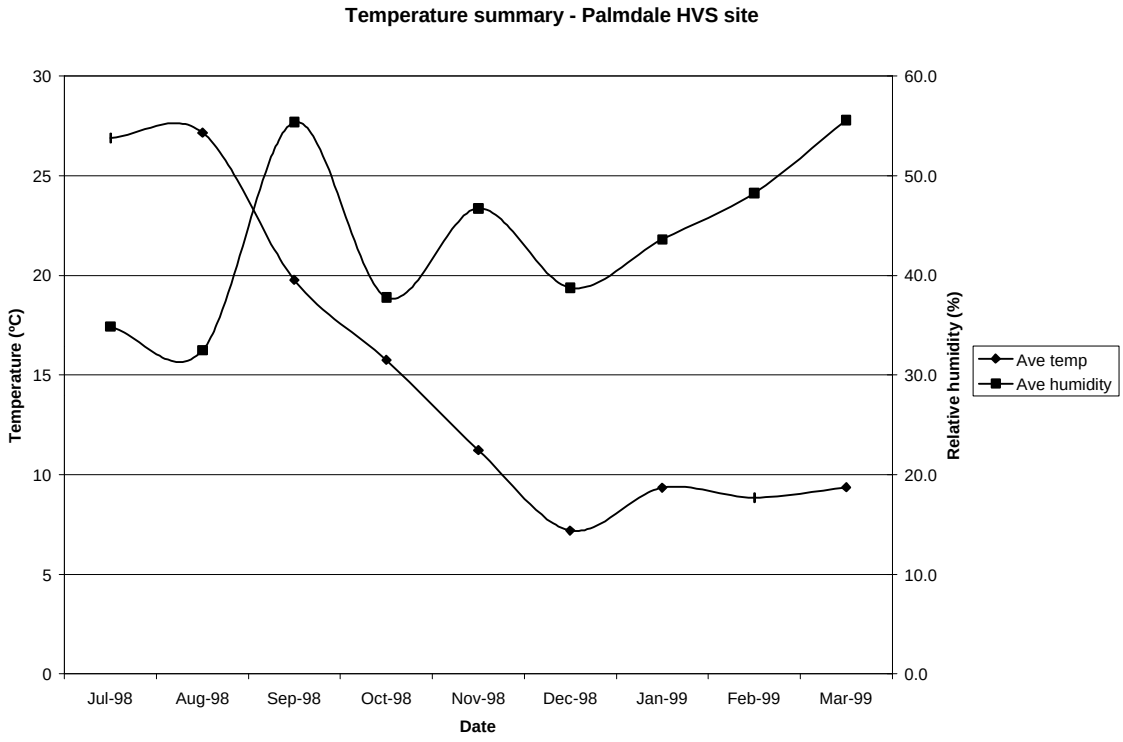

Figure 3.3. Average temperature and humidity at Palmdale HVS site.

The decrease in temperatures and increase in rainfall during the winter months can be seen in the data. The temperature changes can affect the thermal stresses in the concrete slabs while the rainfall and humidity shrinkage of the concrete.

3.4 In-slab temperatures

The temperatures in selected slabs were measured using thermocouples installed at different depths in the slabs during construction. Figure 3.4 shows a multi-depth thermocouple before placement of the concrete slab. The thermocouple wire is supported on a wooden dowel which was driven into the base material.

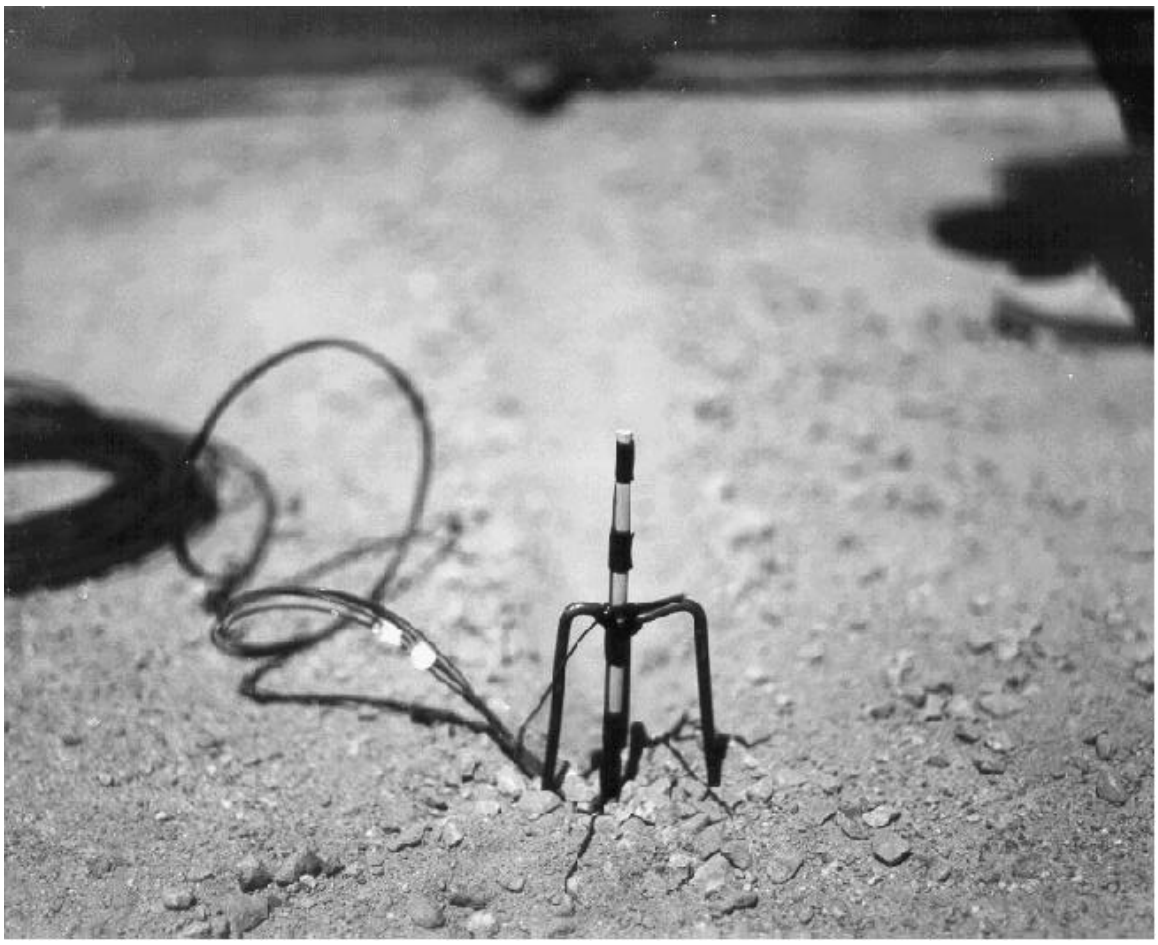

Figure 3.4. Thermocouple prior to placement of concrete.

Thermocouples were installed in section 5 on the south tangent and sections 7, 9, and 11 on the north tangent sections. The slab thickness for these four sections was 200 mm. The temperatures were recorded every two hours with automatic data acquisition units. The thermocouples were installed at the center, edge or corner of the slab, but no significant difference was found between the data from the different locations. All data on the north tangent appeared consistent while the south tangent temperature data was slightly different, possibly because of different exposure at different times of the day.

3.4.1 Temperatures during and immediately after construction

The slab temperatures during and immediately after construction can be used to determine the thermal contraction of the slab, which will result in axial and curling stresses. Results from thermocouple #59 placed in the center of a slab on the south tangent are shown in Table 3.4 and Figure 3.5 below.

Table 3.4. Temperatures after construction for thermocouple 59.

	Temperatures at specified depth (^{o}C)			
	0 mm	**100 mm**	**200 mm**	**Ave**
Max immediately after construction	39.9	40.0	36.2	39.0
Max after 1 day	35.0	30.6	31.4	30.6
Min after 1 day	15.9	23.7	25.2	22.5

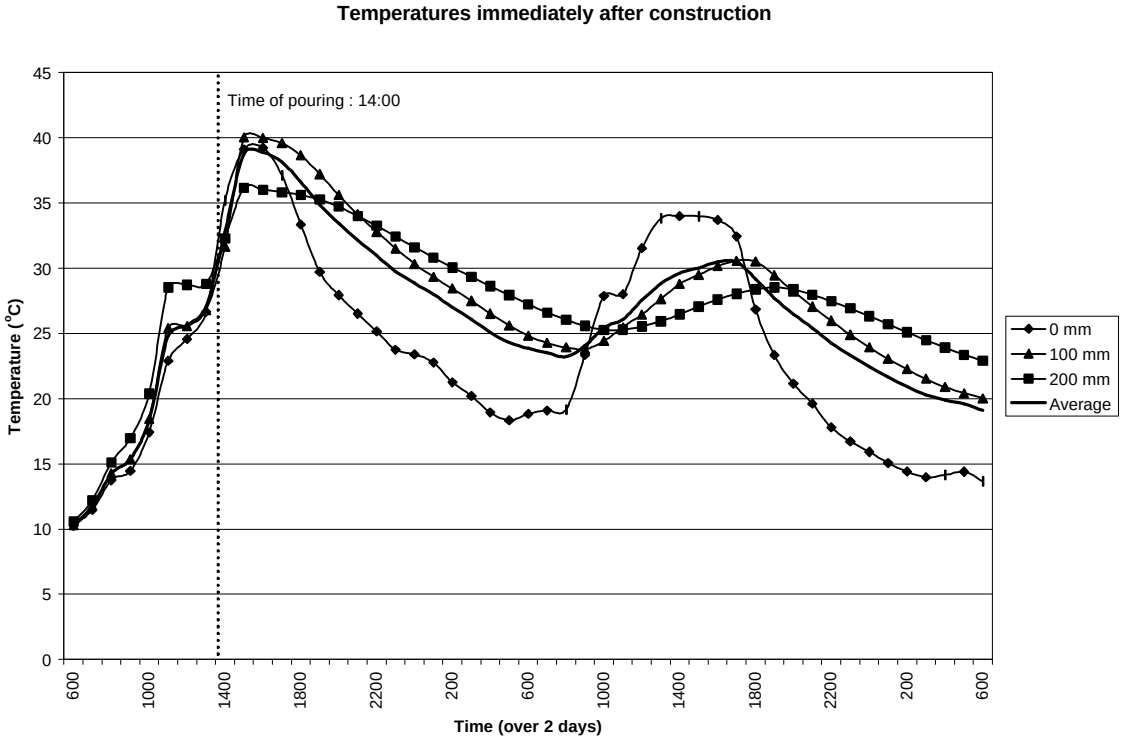

Figure 3.5. Temperature changes during and immediately after construction.

As shown above, the temperatures were fairly uniform through the slab immediately after construction because of the heat generated from the hydration reaction. These temperatures decreased after the first day and typical temperature gradients began developing. The time at which the maximum and minimum temperatures occurred varied through the slab.

One concern of concrete pavement construction is warm weather paving. The temperature and temperature gradient at which a slab sets can result in residual axial and bending stresses. The maximum temperature gradient through the slab on the day of construction was approximately 4.5^{o}C and occurred at approximately 16:00, two hours after pouring which was probably close to the concrete final set time.

3.4.2 Temperatures after construction

The average slab temperatures during the months after construction are illustrated in Figure 3.6, along with the average air temperatures from Figure 3.3.

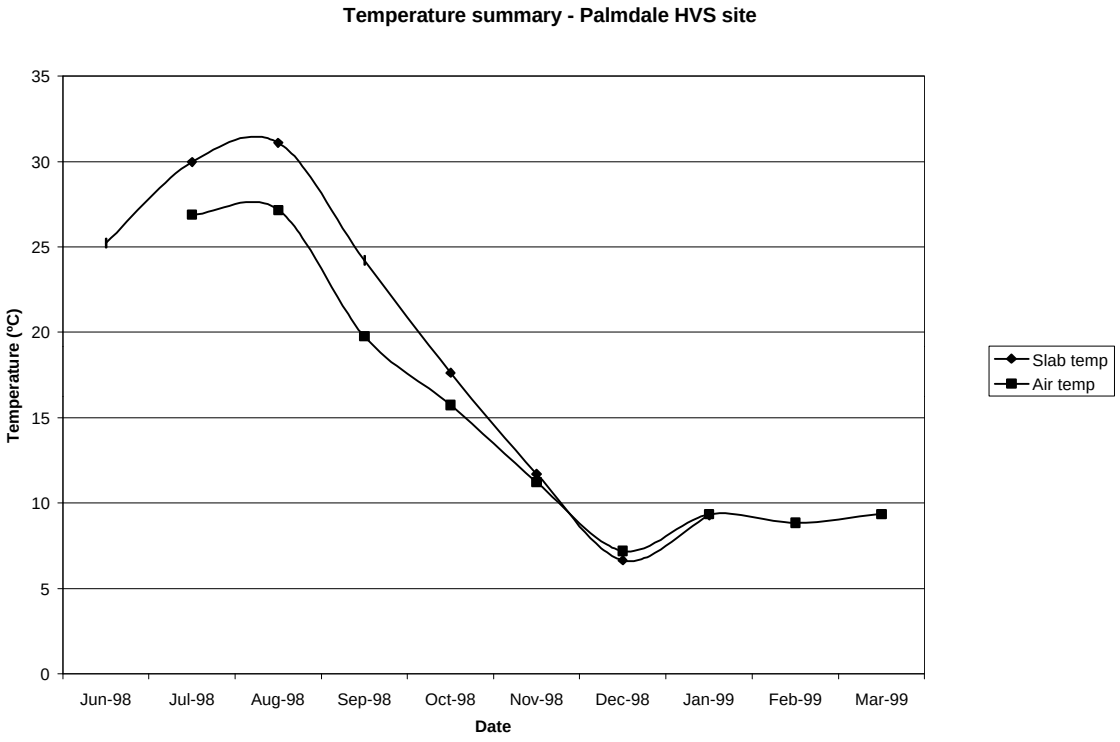

Figure 3.6. Average slab and air temperatures.

As shown in Figure 3.6, the slab temperatures follow the trend of the air temperatures, but are slightly higher, particularly in summer when the slabs will receive more sunlight thereby increasing slab temperature.

The frequency distribution of the slab's temperature gradient from the time of construction until the middle of October 1998 is given in Table 3.5 and Figure 3.7. The frequency distributions for the slab's temperature gradient are separated into the north and south tangent results and into the temperature gradient though the whole slab and the temperature gradient in the top 50 mm of the slab. A positive temperature gradient occurs when the top of the slab is warmer than the bottom and a negative gradient occurs when the bottom is warmer than the top. The whole slab temperature gradient was

calculated assuming a linear distribution of temperature with depth.

Table 3.5. Temperature gradient frequency distribution.

Gradient interval (°C/m)	Whole slab		Gradient interval (°C/m)	Top 50 mm	
	South	North		North	South
110 : 100	0.0	0.0	200 : 180	0.0	0.0
100 : 90	0.0	0.1	180 : 160	0.0	0.7
90 : 80	0.0	0.9	160 : 140	0.0	2.7
80 : 70	0.4	2.7	140 : 120	1.1	3.4
70 : 60	2.7	3.7	120 : 100	4.9	3.3
60 : 50	5.1	3.5	100 : 80	5.1	6.5
50 : 40	5.1	2.4	80 : 60	7.9	4.3
40 : 30	5.2	4.1	60 : 40	6.0	2.2
30 : 20	6.5	5.3	40 : 20	4.7	2.3
20 : 10	6.2	5.1	20 : 0	5.4	4.1
10 : 0	5.8	5.7	0 : -20	6.2	9.4
0 : -10	8.6	9.7	-20 : -40	30.2	23.2
-10 : -20	18.0	17.6	-40 : -60	26.0	25.0
-20 : -30	28.0	22.7	-60 : -80	2.6	11.9
-30 : -40	8.2	14.2	-80 : -100	0.1	1.1
-40 : -50	0.3	2.2	-100 : -120	0.0	0.0
-50 : -60	0.0	0.0	-120 : -140	0.0	0.0

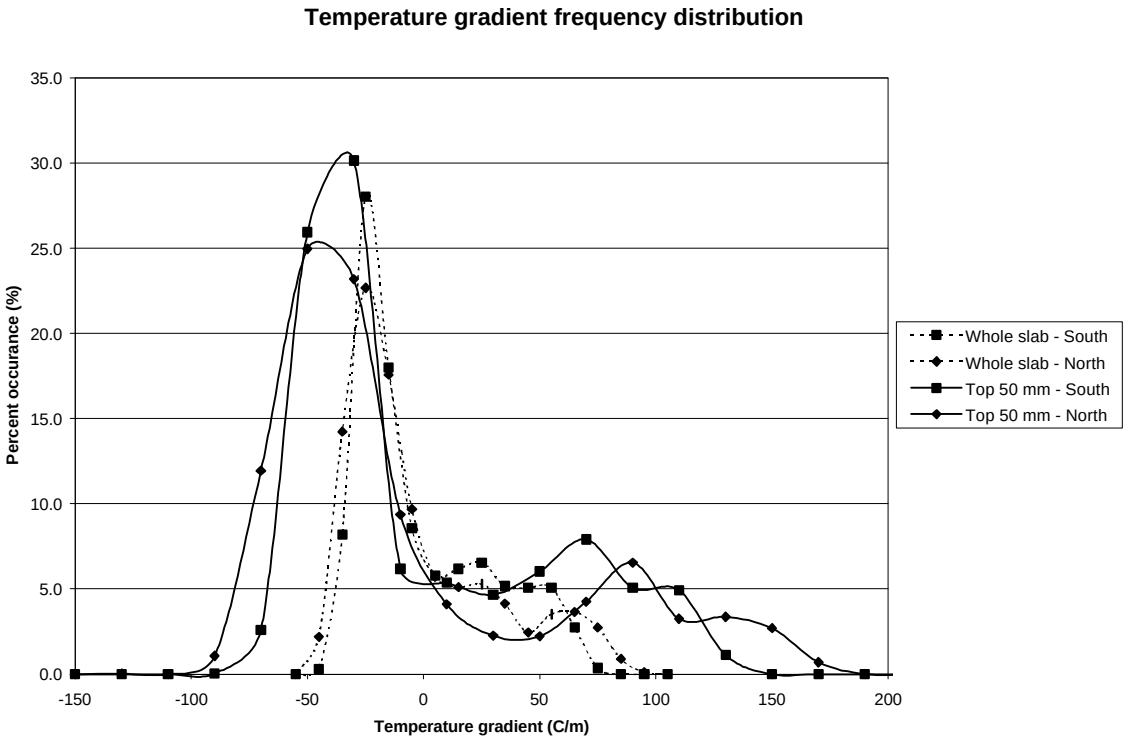

Figure 3.7. Temperature gradient frequency distribution.

The extreme temperature gradients are important in calculating the maximum stresses in a concrete slab. The worst case situations for the greatest positive and negative temperature gradient in the top 50 mm and through the whole slab were all obtained on the south tangent. The temperatures through the slab during these situations are given in Table 3.6 and Figure 3.8. The worst case positive temperature gradient for the whole slab occurred at the same time as the worst case temperature gradient for the top 50 mm of the slab.

Table 3.6. Extreme temperature gradient data.

	Greatest positive gradient		Greatest negative gradient	
	Whole slab	**Top 50 mm**	**Whole slab**	**Top 50 mm**
Date	7/6/98	7/6/98	8/17/98	8/31/98
Time	14:00	14:00	4:00	18:00
Gradient (^{o}C /m)	91.61	176.28	-48.55	-126.94
Depth (mm)	**Temperature (^{o}C)**			
0	44.67	44.67	19.05	25.71
50	35.86	35.86	23.06	32.06
100	32.81	32.81	25.01	34.19
150	28.08	28.08	27.41	34.76
200	26.35	26.35	28.76	33.75

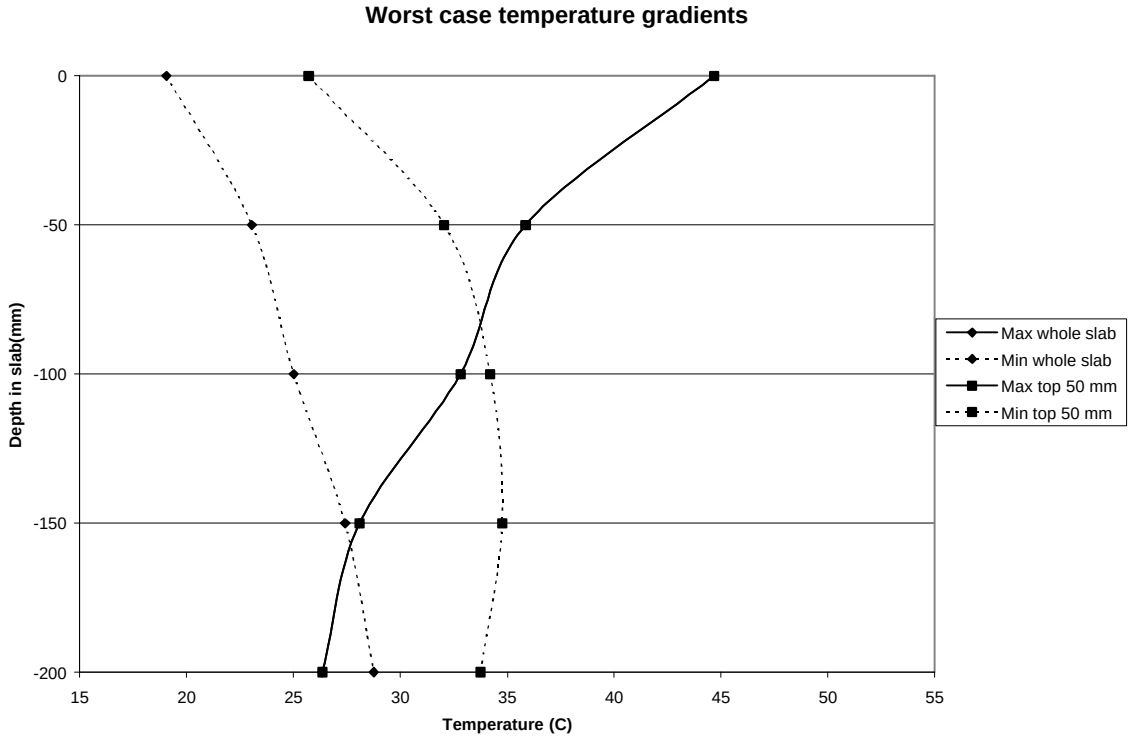

Figure 3.8. Extreme slab temperature distributions.

As can be seen from the data, the extreme positive gradients occurred at 14:00 during the heat of the day. The extreme negative gradient for the whole slab occurred at 4:00 am when the surface of the slab had cooled during the night. The extreme negative gradient for the top 50 mm of the slab occurred at 18:00 on a hot day after a heavy rain shower had rapidly cooled the concrete surface.

3.5 Thermal strains

The daily thermal strains were assessed using data from Carlson A-8 strain gages and from Joint Displacement Measuring Devices (JDMDs) connected to the automatic data acquisition units. The A-8 gages and JDMDs are shown in Figures 3.9 and 3.10.

Figure 3.9. Carlson A-8 strain gage before construction.

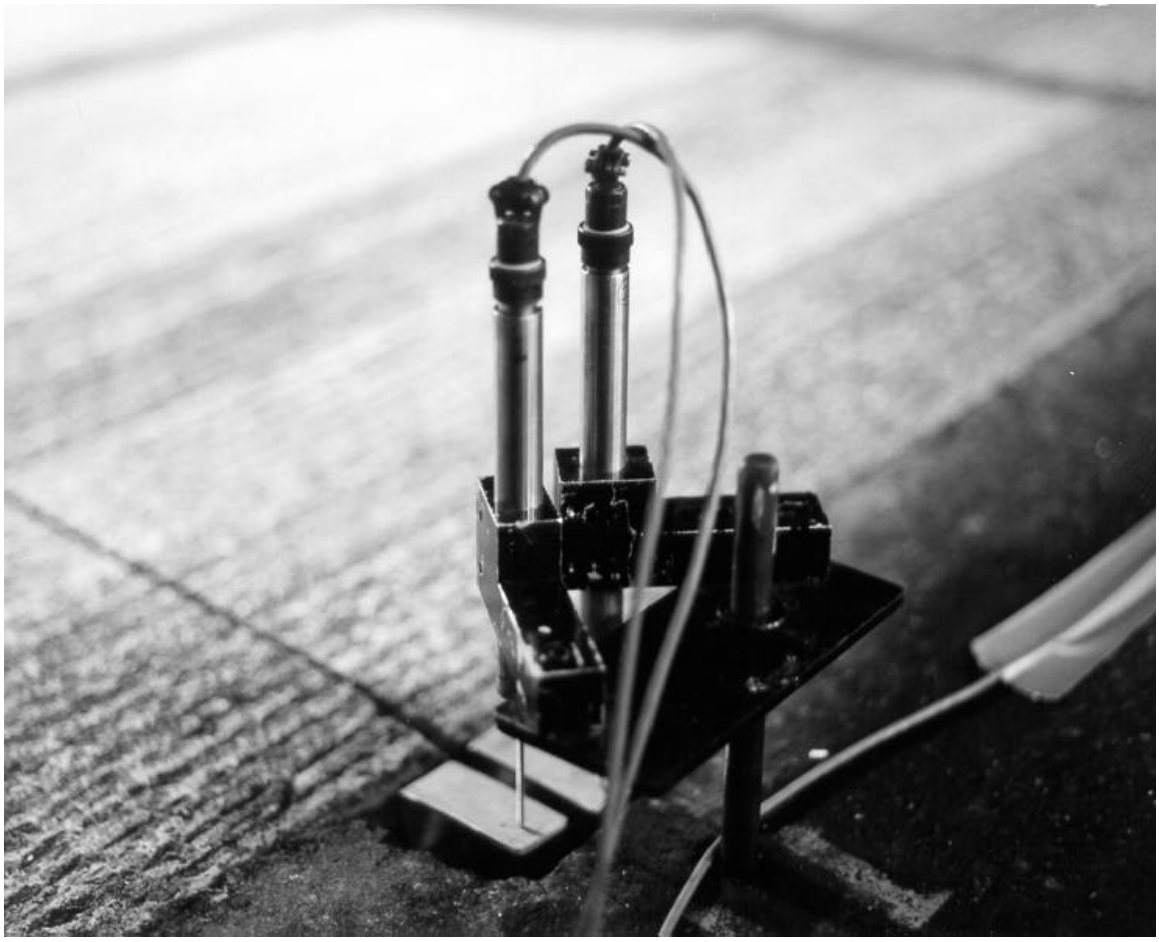

Figure 3.10. Joint displacement measuring device (JDMD).

The change in strain in the Carlson A-8 strain gages and the vertical displacement measured by the JDMDs for a typical day are shown in Figures 3.11 and 3.12. A plot of the A-8 and JDMD data verses slab temperature gradient is shown in Figure 3.13. One of the test sections had a JDMD installed measuring horizontal movements. It was found that this axial movement was significantly lower than the vertical movement, as shown in Figure 3.14.

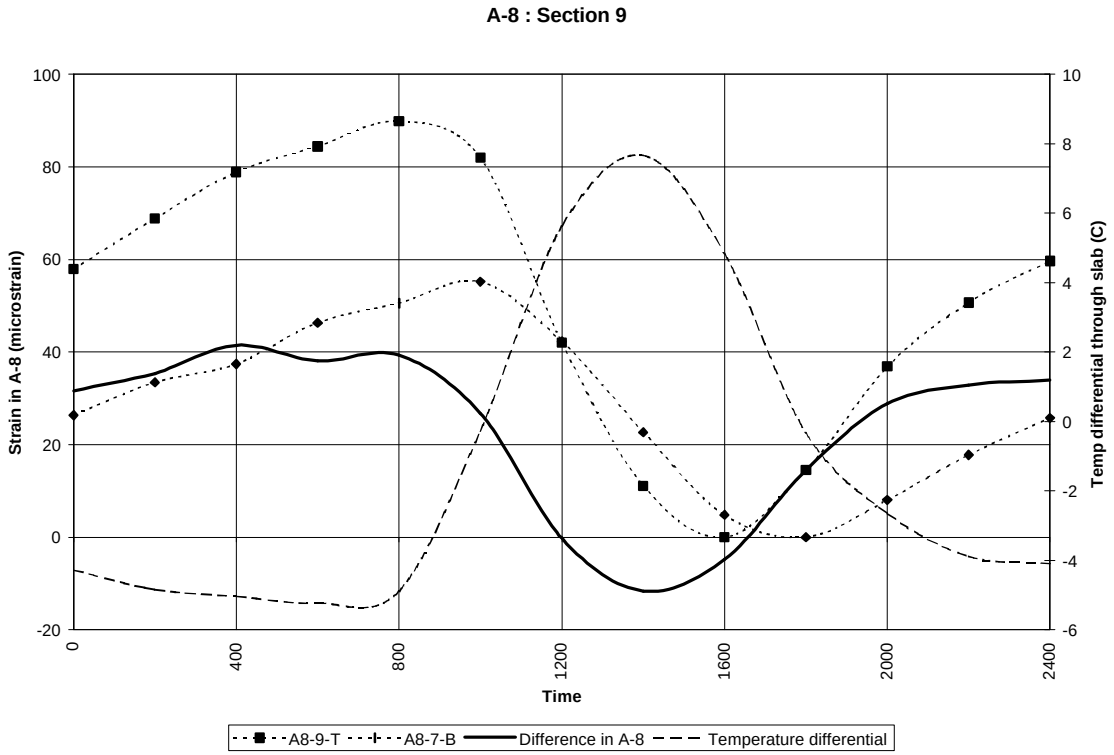

Figure 3.11. Carlson A-8 strain during typical day.

As shown in Figure 3.11, the A-8 readings follow the slab temperature gradient. The readings lag slightly behind the temperature gradient change, probably as a result of the non-linear nature of the temperature gradient. The differential strain between the top and bottom of the slab will result in curling. Figure 3.11 shows the gages are mostly in compression except for a few hours in the afternoon. This indicates the slab is in a permanent curled up position, i.e., there are residual tensile stresses at the top of the slab.

It should be noted that the difference shown in Figure 3.11 is the difference in readings from the gages installed 38 mm from the top and bottom of the slab respectively. The values should be increased if the differential strain between the top and bottom of the slab is required.

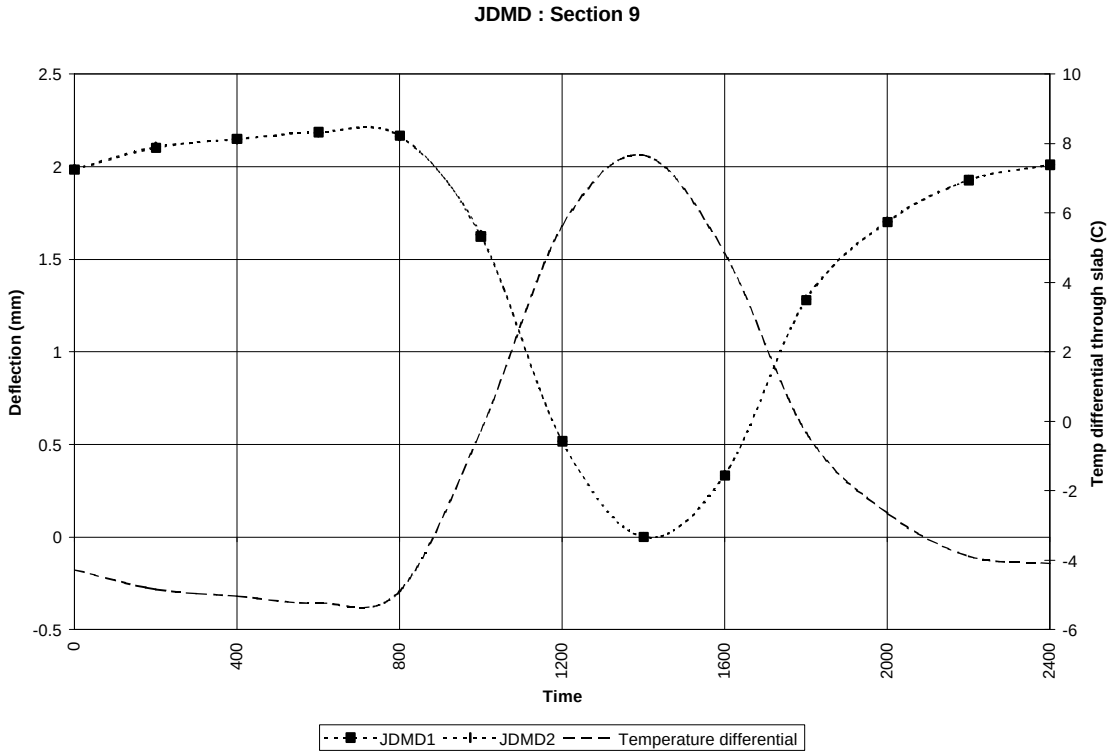

Figure 3.12. JDMD vertical joint displacement during typical day.

JDMDs installed on sections 5, 9 and 11 measured vertical displacements of approximately 2.5 mm during a typical day, while the JDMD installed on section 7 had movements of approximately 0.6 mm. No reason for the low deflections on section 7 could be found, although it could be because the slab in section 7 was either cracked or partially restrained against movement.

The Westergaard and Bradbury thermal stress analyses (Section 2.2.1.1) assume that the slabs do not lift off the base and that full contact is maintained. However, both the JDMD readings and the differential strain between the top and bottom A-8 gages indicate that the slab corners lift-off the base under temperature loading. The measured

corner displacements in Figure 3.12 show the slab was probably not in full contact with the base in the day in question, even when the corner displacements are at a minimum at 14:00 (maximum daytime temperature differential). If the corner was in contact with the base, the JDMD readings would have a flat section where there was no differential movement between the slab and base.

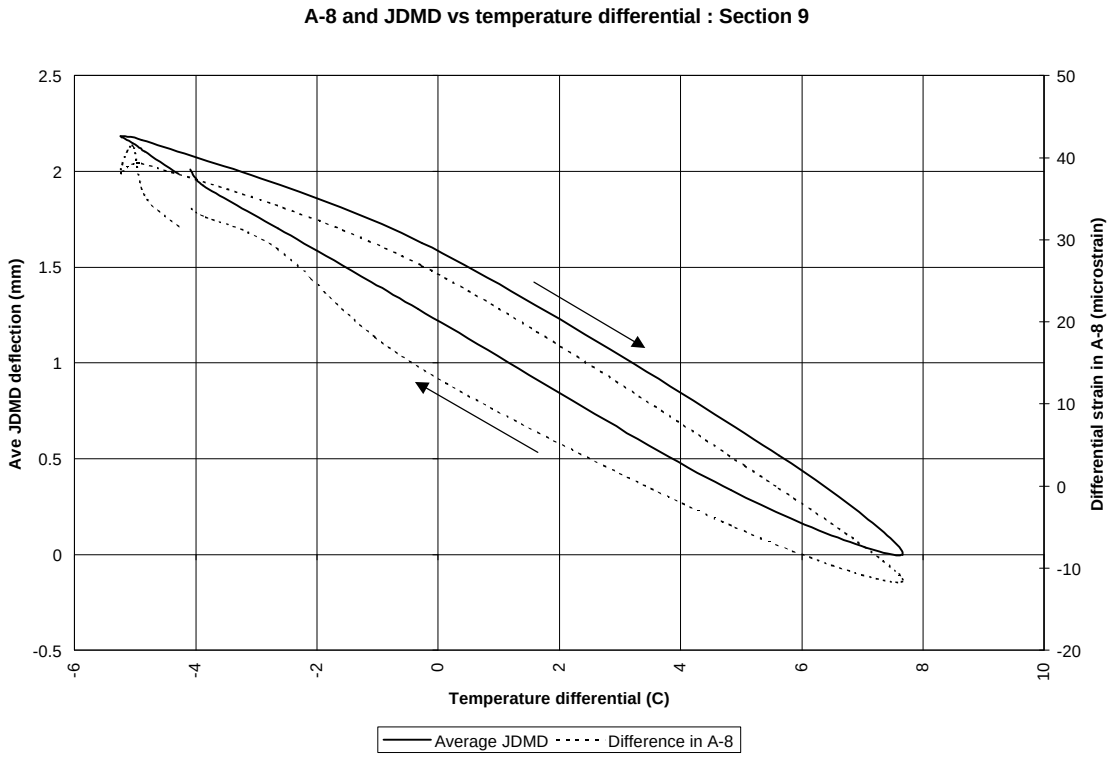

Figure 3.13. Carlson A-8 and JDMD data vs slab temperature gradient.

The change in A-8 and JDMD reading with slab temperature differential during a typical daily cycle can be seen in Figure 3.13. As shown, there is a slight hysteresis to the data, probably as a result of the non-linear nature of the temperature gradients.

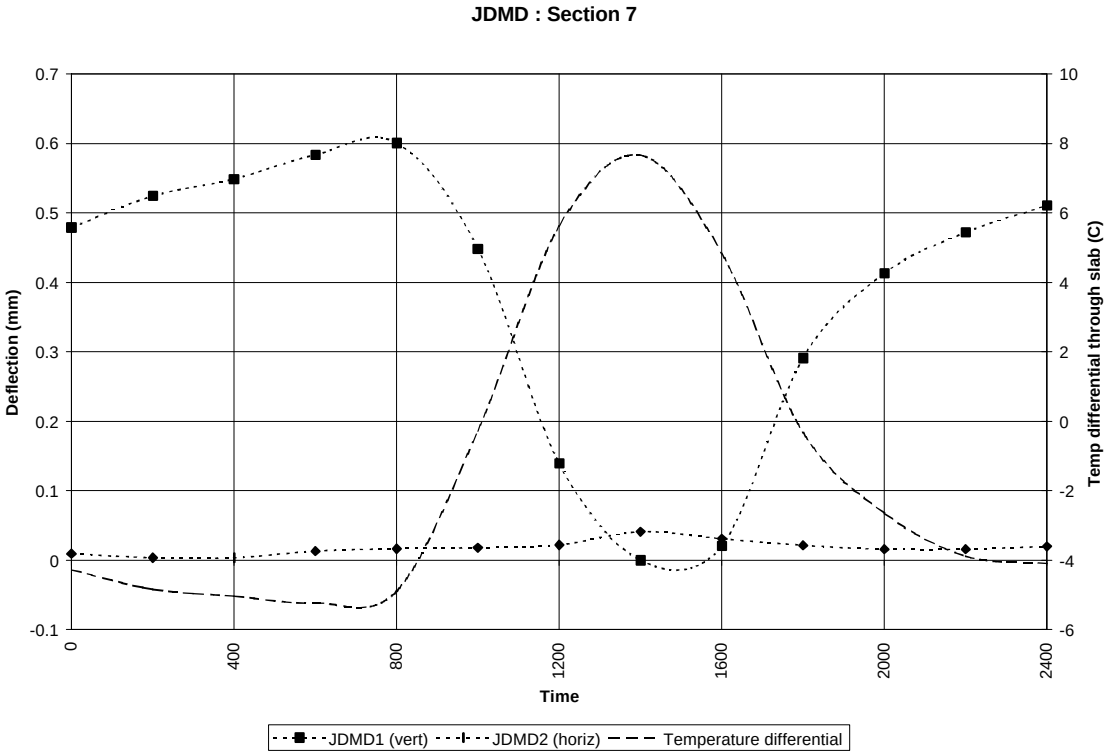

Figure 3.14. Difference in vertical and horizontal joint movement during typical day.

Figure 3.14 illustrates the difference between the vertical and horizontal slab movements during a daily temperature cycle. As shown, the horizontal (axial) movements are significantly lower than the vertical movements. It should be noted that this data is for the JDMDs installed on Section 7 where the vertical movements were significantly lower than the vertical movements on the other sections. The maximum horizontal movement measured was approximately 0.05 mm which should result in very low axial stresses in the slab (Figure 2.4).

3.6 Drying shrinkage

The slab drying shrinkage was assessed using Carlson A-8 strain gages installed at various locations in the test slabs. The gages were installed near the top or bottom of the slabs at the corner, edge, or center. All the instrumented slabs were 200 mm thick.

The average shrinkage at the top and base of the slab and the difference between the top and base shrinkage (the differential shrinkage that will result in curling) are shown in Figure 3.15.

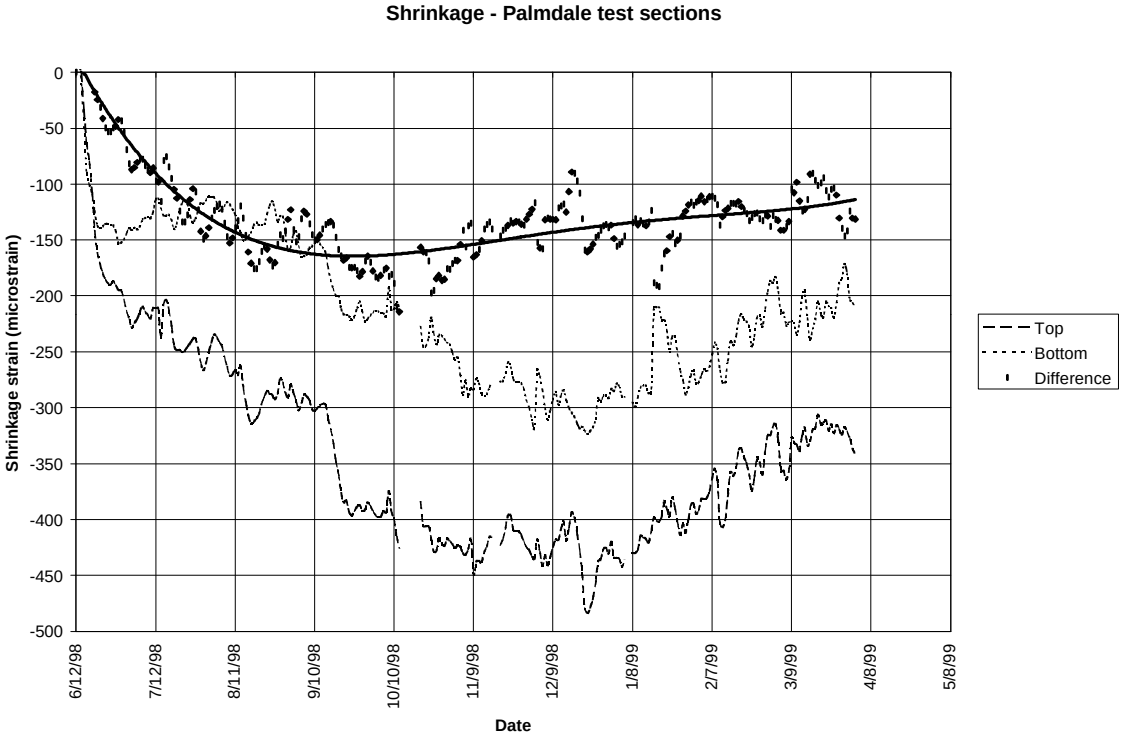

Figure 3.15. Average shrinkage of top and bottom of concrete test sections.

The data shown in Figure 3.15 is the average from all the gages. The gages were installed 38 mm from the top and bottom of the slab. The shrinkage differential should be increased if the strains between the top and bottom of the slab are required.

There was considerable scatter in the data and as a result no noticeable difference in A-8 data for the center, edge or corner of the slabs or for the long or short slabs could be identified. The only identifiable difference was that between the top and bottom of the slab, shown in Figure 3.15.

As shown in Figure 3.15, there was some shrinkage below mid-depth of the slab which appears to contradict previous findings with rigid pavements constructed using ordinary Portland cement (Rasmussen and McCullough, 1998). This shrinkage, however, can be attributed to thermal contraction as the slab cooled from the maximum heat of hydration during the first few days after construction and again as the slab cooled during the winter months. This aspect is described in more detail in Section 5.

The average shrinkage for the gages installed at the corner, edge and center of the slabs is presented in Figure 3.16. There is considerable scatter in the data and it is difficult to distinguish any trends relating to differences in location.

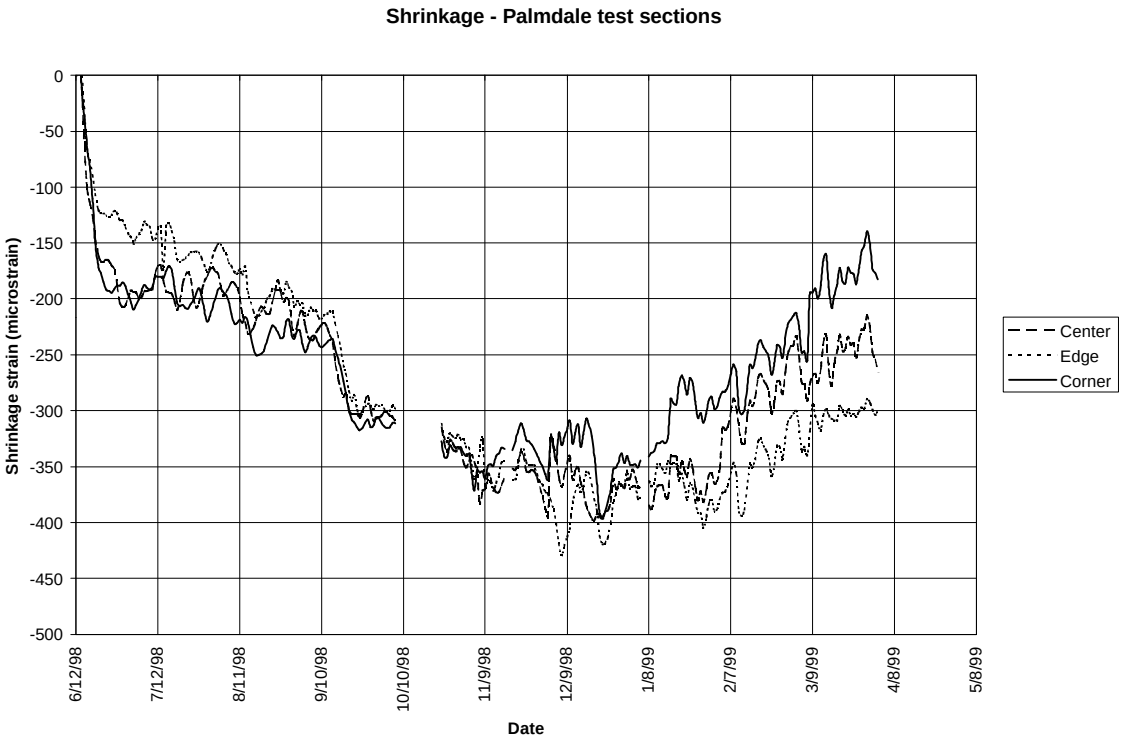

Figure 3.16. Difference in ave shrinkage between corner, edge and center of slabs.

There was no discernable difference between the strains measured in shorter slabs and those measured in longer slabs. There was insufficient data to determine whether the installation of dowels or tie bars had any effect on the measured strains.

3.7 Other instrumentation

Other instrumentation was installed in the test section, but most of this was not permanently connected to data acquisition units. One exception was instrumented dowel bars, as shown in Figure 3.17.

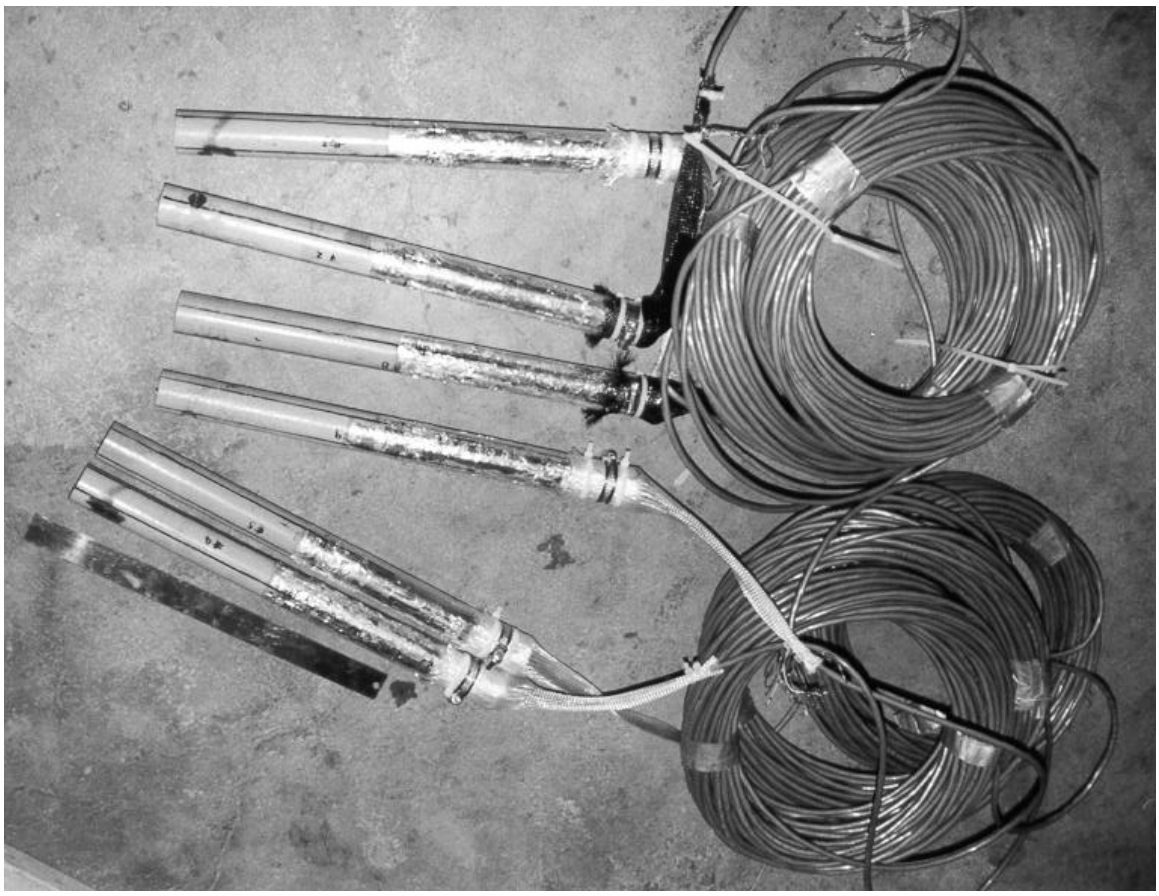

Figure 3.17. Instrumented dowel bars before installation.

These were installed to determine the strains in the dowel bars under environmental and traffic loading. Previous work at Ohio University has indicated that the stresses in the dowel bars can be over 50 percent of the working stress of the steel used for the bars (Sargand, 1999). The data from the instrumented dowel bars was analyzed by researchers at the University of California at Berkeley and at Ohio University. It was found that the data was inconsistent between the different dowels and with previous results and the data was therefore not used in any analysis.

4 LABORATORY TESTING

4.1 Coefficient of thermal expansion

4.1.1 Experimental design

The concrete coefficient of thermal expansion from the Palmdale mix design (cement and aggregates) was determined using two different test methods, ASTM C 531-85 and USACE test method CRD-C 39-81.

For both methods, concrete samples were cast in 76.2 mm x 76.2 mm x 285 mm molds with studs at each end so that changes in length could be accurately measured using a comparator, as shown in Figure 4.1.

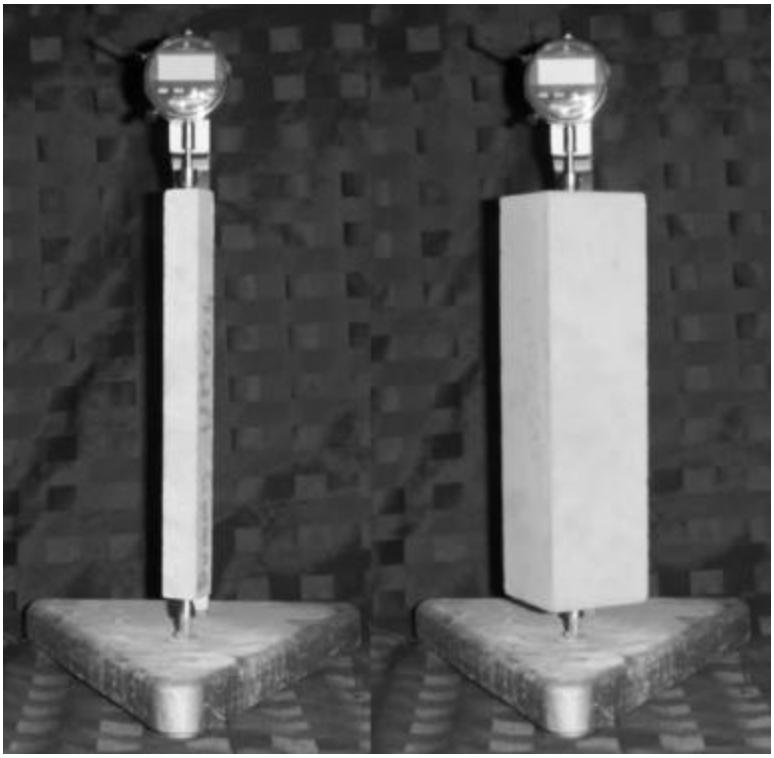

Figure 4.1. Comparator for measuring mortar (left) and concrete (right) beams

Two concrete mix designs were tested, the first was the same mix design used for the construction of test sections in Palmdale (Table 3.1) and the second was a typical Caltrans mix design using Type I/II cement. The aggregates used for the construction of the Palmdale test section (Gabbro coarse aggregate and quartz fine aggregate) were used for both mixes. The mix designs are given in Table 4.1 below.

Table 4.1. Mix designs for the determination of coefficient of thermal expansion.

Material	FSHCC mix (Palmdale)		Caltrans mix	
	% dry agg mass	kg/m^3 concrete	% dry agg mass	kg/m^3 concrete
Coarse aggregate	56.8	1116	56.8	1156
Fine aggregate	43.2	849	43.2	879
Type I/II cement	4.4	86	17.9	364
C$\bar{s}$A cement	17.7	348	-	-
Water	11.1	218	9.4	191
Delvo ® stabilizer	0.213	4.2	-	-
Micro Air ® air entrainment	3.0 x 10^{-3}	59 g/m^3	3.2 x 10^{-3}	65 g/m^3

In both cases, a water to cement ratio of 0.45 was used as previous research had indicated that this factor does not have a significant effect on the coefficient of thermal expansion (Tia et al, 1991).

Three replicates were performed for each test. The coefficient of thermal expansion was measured after curing at 20^{o}C either under water or in a temperature controlled room with a relative humidity of approximately 40 percent. Both 28 day and

90 day curing times were used. The samples were discarded after testing at 28 days and different samples were used for the 90 day testing.

4.1.2 Test methods

4.1.2.1 ASTM test method

There is no ASTM standard test for determining the coefficient of thermal expansion of concrete. ASTM C 531-85 was developed for the determination of linear shrinkage and the coefficient of thermal expansion of mortars, grouts and monolithic surfacings and this was slightly modified to determine the coefficient of thermal expansion of concrete. The test involves measuring the length of a small concrete beam after being placed in a room at 22^{o}C, after being heated in an oven to 100^{o}C for 24 hours, and again after being placed in the 22^{o}C room for 24 hours. The samples were oven dried at 100^{o}C for 3 days before testing in order to reduce the effect of drying shrinkage, particularly for the water-cured samples. The coefficient of thermal expansion is determined by dividing the change in length by the change in temperature.

4.1.2.2 USACE test method

The USACE test method CRD-C 39-81 uses similar principles as the ASTM method with the exception that the samples are first cooled to 5^{o}C under water and then heated to 60^{o}C in a water bath before returning them to 5^{o}C under water. For this test the samples were placed under water for four days before testing to reduce the effect of concrete drying shrinkage reversal on the measurement of the coefficient of thermal expansion.

4.1.3 Test results

The average test results for the three replicates are presented in Table 4.2.

Table 4.2. Results of coefficient of thermal expansion testing.

Mix design	Curing time (days)	Curing condition	Test type	Coefficient of thermal expansion	
				(1/^{o}C)	% Ave
FSHCC (Palmdale)	28	Water	ASTM	6.82E-06	84
			USACE	8.17E-06	100
		Air	ASTM	8.07E-06	99
			USACE	8.89E-06	109
	90	Water	ASTM	7.15E-06	88
			USACE	8.59E-06	106
		Air	ASTM	7.50E-06	92
			USACE	9.05E-06	111
Caltrans	28	Water	ASTM	7.91E-06	97
			USACE	7.99E-06	98
		Air	ASTM	8.25E-06	101
			USACE	8.80E-06	108
	90	Water	ASTM	8.03E-06	98
			USACE	8.71E-06	107
		Air	ASTM	8.50E-06	104
			USACE	7.88E-06	97
Average of tests on FSHCC mix (as used in Palmdale)				*8.03E-06*	*99*
Average of tests on Caltrans mix				*8.26E-06*	*101*
Average of all tests				*8.14E-06*	*100*

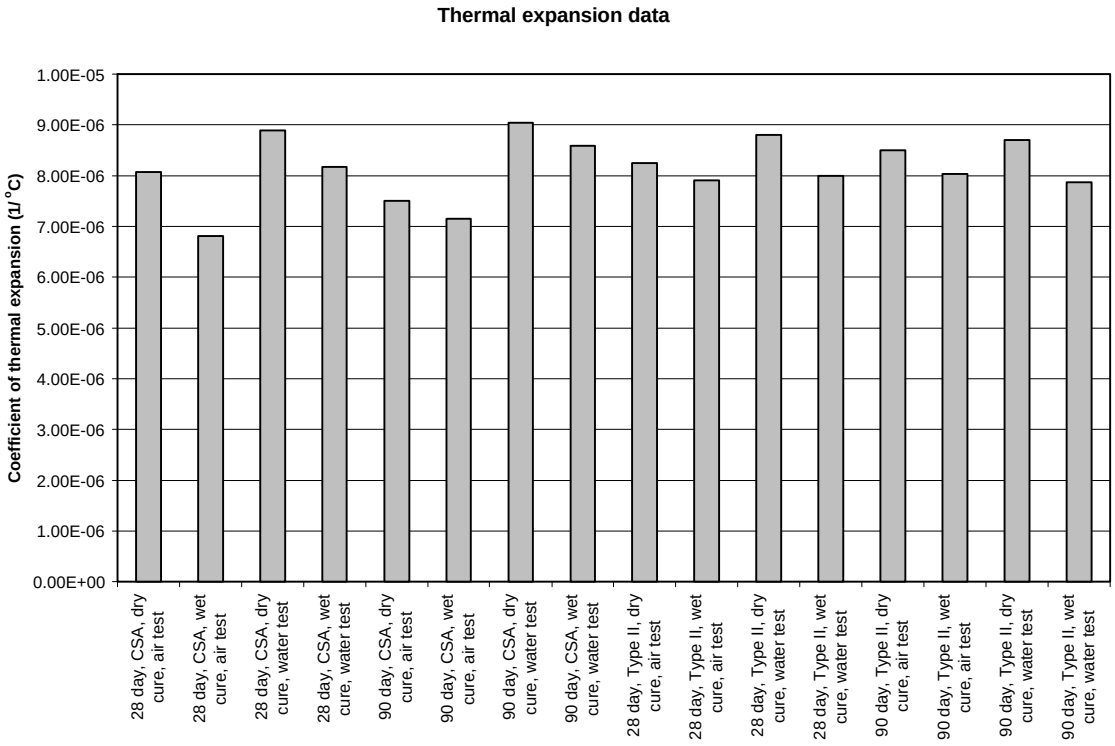

Figure 4.1. Results from coefficient of thermal expansion testing.

The average coefficient of thermal expansion of the concrete tested is slightly below typical values for concrete (Rasmussen and McCullough, 1998, Tia et al, 1991).

The results in Table 4.2 were analyzed and it was found that the USACE test method (under water heating and cooling) generally gives a higher coefficient of thermal expansion (α) than the ASTM method (heating and cooling in air). The air-cured specimens have a higher α than the water cured specimens. Previous research has shown that α for concrete is more sensitive to the α of the aggregates and the mix proportions (Rasmussen and McCullough, 1998, Tia et al, 1991). Both mixes had the same aggregates and similar mix proportions.

The α for the Gabbro coarse aggregate is typically between 5.5E-06 and 8.0E-06

while that for the quartz fine aggregate is typically between 10.0E-06 and 12.0E-06 (Tia, et al, 1991).

Previous research (Meyers, 1951) noted that α of cement mortar is at a maximum when the sample is at 70 percent relative humidity and at a minimum at 100 percent relative humidity and below 40 percent relative humidity.

The curing times of 28 and 90 days appeared to have no effect on the coefficient of thermal expansion for either mix. The two mix designs have little effect on the coefficient of thermal expansion. These slight variations in the coefficient of thermal expansion for the different curing conditions and test type are similar to those noted by researchers in Florida (Tia et al, 1991).

As the coefficient of thermal expansion for the Palmdale concrete is similar to that of concrete containing the same aggregates and Type II Portland cement (see previously), it is unlikely that the mix design used in Palmdale resulted in thermal cracking that would not have occurred with another cement. Because the measured coefficient of thermal expansion for the Palmdale mix was lower than that typically measured for concrete, it is likely that the thermal effects were less significant than they would be for typical mixes.

4.2 Shrinkage

4.2.1 Experimental design

To determine if shrinkage of the concrete was the predominant reason why the concrete pavements cracked, the cement used in Palmdale was checked against several

other commercially available cement types. Three different methods of assessing drying shrinkage were used. The first and second involved measuring the shrinkage of cement mortar according to ASTM C 596-96 and California Test CT 527, respectively. The third measured the shrinkage of small concrete beams according to a slightly modified version of ASTM C 157-93.

The samples were measured after curing for 7, 14, 21, 28 and 90 days. Three different curing conditions were used:

1. In a humidity cabinet at 20^{o}C and 50% relative humidity

2. In a temperature controlled room at 20^{o}C and between 30 % and 50 % relative humidity

3. In a lime saturated water bath at 20^{o}C.

25 mm x 25 mm x 285 mm molds were used for the mortar bars and 76.2 mm x 76.2 mm x 285 mm molds were used for the concrete specimens.

4.2.2 Test methods

All three test methods involve measuring the length change of the samples using a comparator at different times after mixing.

4.2.2.1 ASTM mortar bar shrinkage test

ASTM C 596-96 was slightly modified for this testing. Water to cement ratios of both 0.40 and 0.50 were used instead of the one water to cement ratio required by the test method. The water to cement ratio in the ASTM test method is determined from the flow

of the mortar. A blend of 80 % CS̄A cement and 20 % Type II cement was used, as this was the blend used in the construction of the Palmdale test sections. The same Type II cement used in Palmdale was used as a reference. No admixtures were used in this testing. Since the CS̄A blend had a set time of only a few minutes, the mix water and sand were chilled before mixing to delay the initial set time. The CS̄A samples were removed from the molds 8 hours after mixing and the Type II cement samples were removed from the molds 24 hours after mixing. This was found not to have any significant influence on the results (see Section 4.2.3). After removal from the molds, the samples were placed under water at 20^{o}C for three days from the time of mixing and then an initial reading was taken. The samples were then transferred to the three curing locations. Three replicates were performed for each test level.

4.2.2.2 California mortar bar shrinkage test

California Test CT 527 uses the same mixing and casting procedures as used for ASTM C 596-96 with the exception the water to cement ratio is specified as 0.375 for Type II cement and as 0.39 for Type III cement. A total of eight different cement types were tested (see Table 4.4). A water to cement ratio of 0.39 was used for the seven fast setting cements and the specified water content of 0.375 was used for the Type II cement. The samples were removed from the molds at 8, 12 or 24 hours after mixing and placed under water at 20^{o}C for 30 minutes to adjust the sample to the standard temperature. The samples were then measured to get an initial length reading and then returned to the water bath o determine the water expansion of the samples. After measuring the expansion at three days after mixing, the samples were transferred to the humidity cabinet at 20^{o}C and

50% relative humidity. Four replicates were performed for each test level, as per the test method.

4.2.2.3 ASTM concrete shrinkage test

The concrete mix designs for ASTM C 157-93 were similar to those used for the thermal expansion test samples (Table 4.1). The only difference was that water cement ratios of 0.40 and 0.50 were used. Because of space restrictions, the concrete beams were not cured in the humidity cabinet but in the temperature-controlled room or under water.

4.2.3 Test results

The summarized test results from the shrinkage tests are presented in Tables 4.3 to 4.6 and Figures 4.2 to 4.5.

4.2.3.1 ASTM mortar bar shrinkage test

The shrinkage of mortar bars made with a Type II cement and the C$\bar{s}$A cement blend used in the construction of the Palmdale test sections is summarized in Table 4.3 and Figure 4.2.

Table 4.3. Average shrinkage of mortar bars using ASTM test method.

Curing condition	W/C ratio	Cement type	Ave shrinkage at given curing time (με)				
			3	7	14	28	90
50% RH	0.4	Type II	0	-293	-493	-576	-710
30-40% RH	0.4	Type II	0	-327	-612	-687	-789
Under water	0.4	Type II	0	32	49	67	105
50% RH	0.5	Type II	0	-370	-610	-708	-851
30-40% RH	0.5	Type II	0	-451	-746	-783	-856
Under water	0.5	Type II	0	22	58	54	89
50% RH	0.4	80% C$\bar{s}$A, 20% Type II	0	-835	-1186	-1314	-1319
30-40% RH	0.4	80% C$\bar{s}$A, 20% Type II	0	-981	-1247	-1281	-1288
Under water	0.4	80% C$\bar{s}$A, 20% Type II	0	27	104	168	235
50% RH	0.5	80% C$\bar{s}$A, 20% Type II	0	-1010	-1357	-1470	-1556
30-40% RH	0.5	80% C$\bar{s}$A, 20% Type II	0	-1043	-1348	-1386	-1415
Under water	0.5	80% C$\bar{s}$A, 20% Type II	0	20	56	98	125

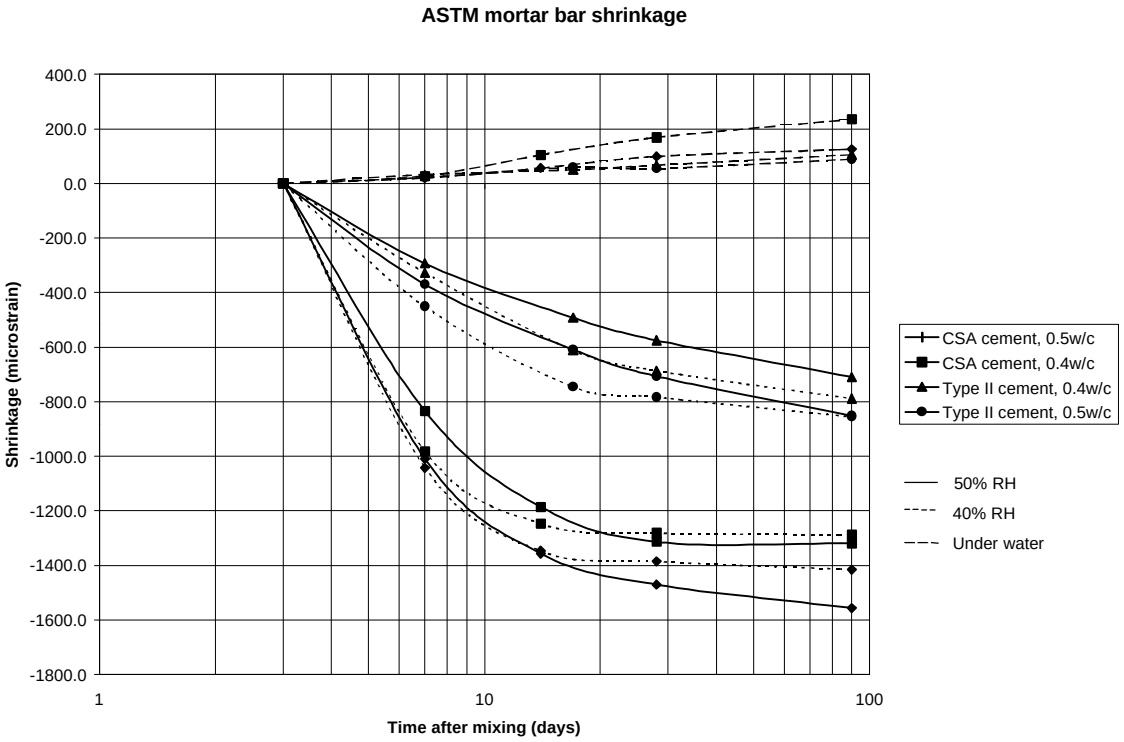

Figure 4.2. Average shrinkage of mortar bars using ASTM test method.

The CS̄A cement used in the Palmdale test sections had a significantly higher shrinkage than the Type II cement at all curing times and types. The CS̄A cement tested had 185 percent more drying shrinkage at 7 days than the Type II cement at a w/c ratio of 0.40. The samples stored at approximately 40 percent relative humidity (uncontrolled) had a higher initial shrinkage than those stored at a controlled 50 percent relative humidity, but this trend did not hold with time. The samples mixed at a water to cement ratio of 0.50 had higher shrinkage than those mixed at a water to cement ratio of 0.40. The samples stored under water expanded with time, indicating that the shrinkage observed in other specimens was drying shrinkage.

4.2.3.2 Caltrans mortar bar shrinkage test

Shrinkage of different fast setting hydraulic cements was assessed using the Caltrans test method (CT 527). The standard test method was modified to determine whether there would be any difference in the results if the mortar bars were left in the molds for 24 hours (the time in the standard test method) or for 8 to 12 hours (the time before opening FSHCC pavements to traffic).

In addition to the CS̄A cement used in the construction of the Palmdale test sections, two other brands of CS̄A cements (CS̄A1 and CS̄A2) were used, one blended with OPC and chemical additives and the other unblended. CS̄A1 was produced by the same manufacturer as the CS̄A cement used in Palmdale, but as shown later, the two cements had significantly different properties. The Type III cement combined with pozzolan consisted of a Type III with 10% fly ash and 5% silica fume replacement. The Type III with Calcium Chloride ($CaCl_2$) was mixed by replacing some of the mix water with 2 percent $CaCl_2$ by mass of cement. The $CaCl_2$ was at 43 percent concentration.

The W/C ratio was 0.375 for the Type II cement and 0.39 for all other cements, as per the test method.

The results are summarized in Table 4.4 and Figure 4.3.

Table 4.4. Ave shrinkage of mortar bars using Caltrans test method.

Cement type	Time in mold (hrs)	Ave shrinkage at given curing time (με)				
		3	7	14	28	90
C$\bar{s}$A2	8	0	-260	-311	-332	-382
C$\bar{s}$A2	24	0	-254	-295	-320	-373
CA	8	0	-484	-590	-650	-678
CA	24	0	-491	-597	-657	-680
90% C$\bar{s}$A1, 10% fly ash	8	0	-308	-462	-528	-578
90% C$\bar{s}$A1, 10% fly ash	24	0	-307	-476	-539	-596
Type III	12	0	-473	-651	-818	-912
Type III	24	0	-440	-628	-798	-876
Type III + 2% $CaCl_2$	12	0	-670	-907	-1036	-1079
Type III + 2% $CaCl_2$	24	0	-655	-882	-1025	-1084
Type III + pozzolan	12	0	-455	-658	-793	-849
Type III + pozzolan	24	0	-441	-641	-786	-844
Type II	24	0	-370	-368	-722	-765
80% C$\bar{s}$A (Palmdale), 20% Type II	24	0	-643	-936	-1112	-1170

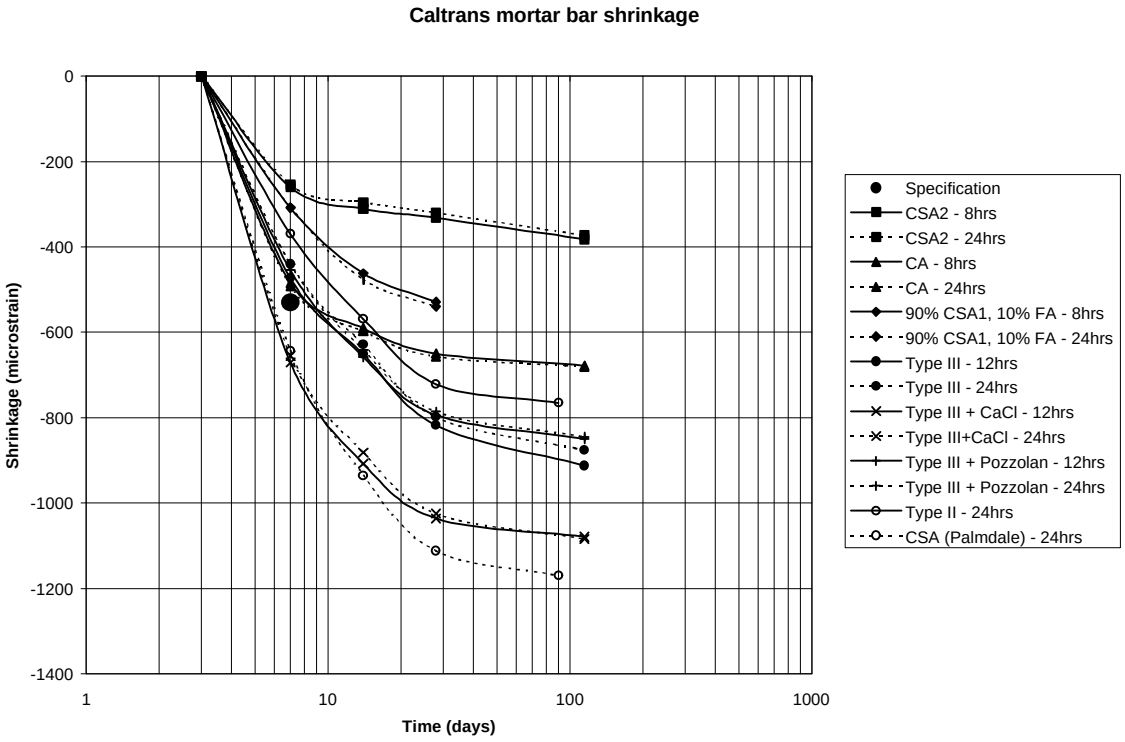

Figure 4.3. Average shrinkage of mortar bars using Caltrans test method.

As shown in Table 4.4 and Figure 4.3, there is no significant difference in the drying shrinkage of the mortar bars if they are left in the mold for 8-12 hours or 24 hours. This is probably because no irreversible plastic shrinkage occurs between 8 and 24 hours. Any reversible shrinkage is overcome by soaking the specimens in water for three days.

Only the CS̄A blend as used in the construction of the Palmdale test sections and the Type III cement with $CaCl_2$ added did not meet the Caltrans specification of a maximum of 530 microstrain for shrinkage. The CS̄A cement used in Palmdale and CS̄A1 with fly ash were made by the same manufacturer yet produced a wide difference in drying shrinkage.

4.2.3.3 ASTM concrete shrinkage test

The drying shrinkage of concrete was assessed with the same mix designs as used in the concrete thermal expansion test (Table 4.1). The results are summarized in Table 4.5 and Figure 4.4.

Table 4.5. Average shrinkage of concrete using ASTM test method.

Curing condition	W/C ratio	Mix design (Table 4.1)	Ave shrinkage at given curing time (με)				
			3	7	14	28	90
30-50% RH	0.4	Caltrans	0	-163	-249	-396	-581
Under water	0.4	Caltrans	0	-42	-34	-40	-30
30-50% RH	0.5	Caltrans	0	-166	-296	-463	-608
Under water	0.5	Caltrans	0	-55	-54	-52	-67
30-50% RH	0.4	FSHCC	0	-243	-389	-577	-799
Under water	0.4	FSHCC	0	-1	44	73	130
30-50% RH	0.5	FSHCC	0	-264	-443	-687	-937
Under water	0.5	FSHCC	0	-5	32	41	78

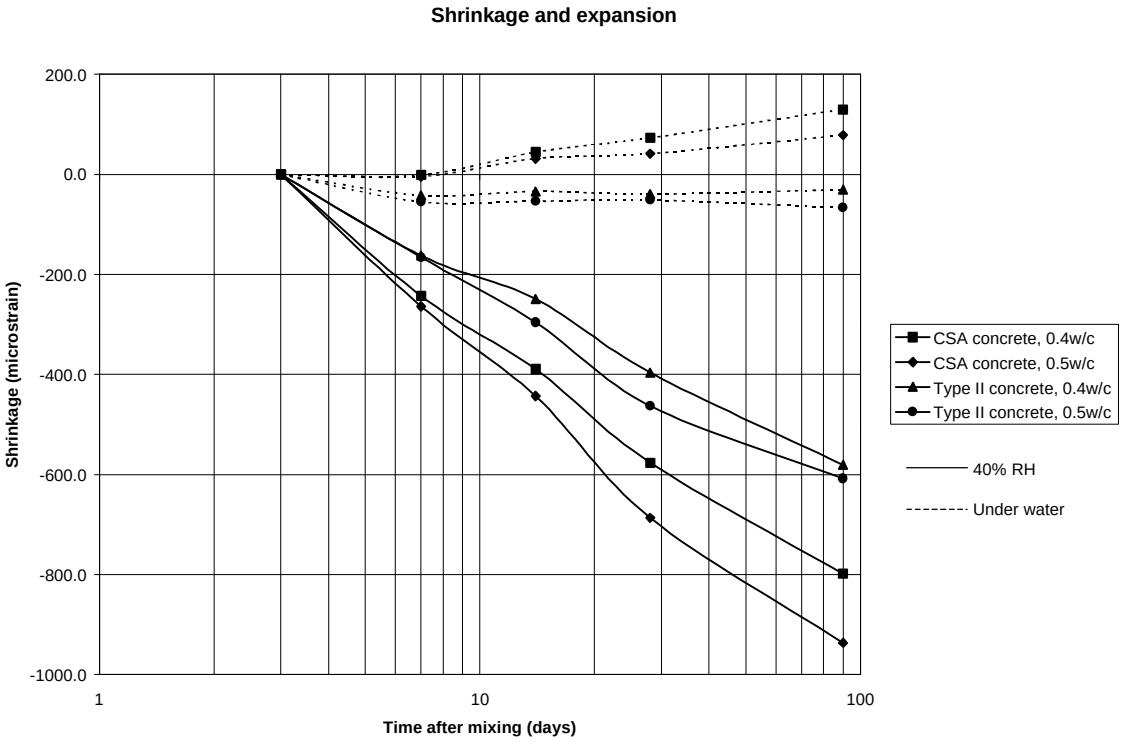

Figure 4.4. Average shrinkage of concrete using ASTM test method.

As shown in Figure 4.4 and Table 4.5, the concrete drying shrinkage was less for lower water to cement ratio for both Type II and C$\bar{s}$A cement. The shrinkage of the concrete made with C$\bar{s}$A cement was significantly higher than that with Type II cement. The drying shrinkage measured during the tests can only be used as a relative comparison of the different cements and concrete as the measurements are for free shrinkage and do not include partial restraint or creep as occurs in the field situation.

4.2.3.4 Caltrans mortar bar expansion test

The expansion of the mortar bars under water is assessed as part of Caltrans test method CT 527. The purpose of the expansion test is to indicate the amount of calcium

sulfate in the cement. This test was original intended for use only in Portland cements where expansion of the mortar bars could be correlated with the amount of calcium sulfates in the cement.

The samples were removed from the molds and placed under water for 30 minutes before measuring, to obtain a baseline reading. They were then measured again after three days under water. The results of the expansion testing are summarized in Table 4.6 and Figure 4.5. The Caltrans specification for maximum permissible expansion is 100 με.

Table 4.6. Average expansion of mortar bars using Caltrans test method.

Cement type	Time in mold (hrs)	Average expansion (με)
C$\bar{s}$A2	8	70.1
C$\bar{s}$A2	24	29.8
CA	8	-151.5
CA	24	-3.5
90% C$\bar{s}$A1, 10% fly ash	8	9.6
90% C$\bar{s}$A1, 10% fly ash	24	14.0
Type III	12	58.7
Type III	24	24.1
Type III + 2% $CaCl_2$	12	88.4
Type III + 2% $CaCl_2$	24	29.8
Type III + pozzolin	12	53.4
Type III + pozzolin	24	26.3
Type II	24	10.5
80% C$\bar{s}$A (Palmdale), 20% Type II	24	55.2

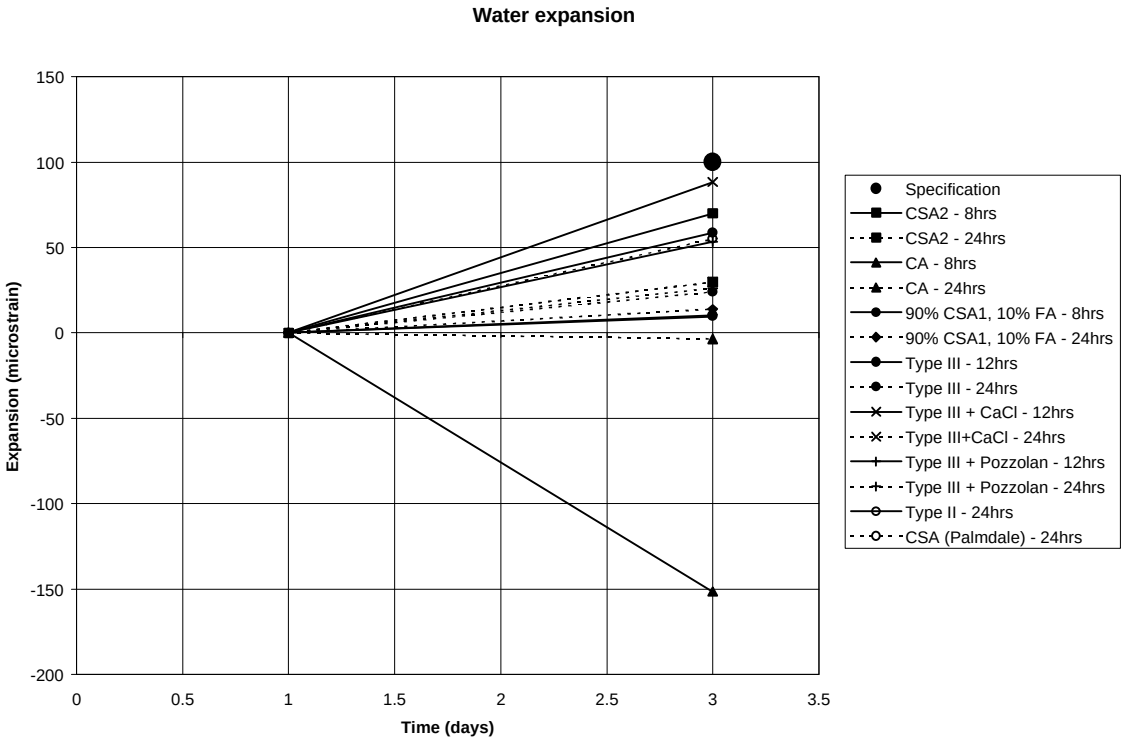

Figure 4.5. Average expansion of mortar bars using Caltrans test method.

As shown in Table 4.6 and Figure 4.5, none of the specimens exceeded the allowable expansion of 100 microstrain. The CA cements samples removed from the mold after 8 hours shrunk an average of approximately 150 microstrain. This can be explained by the hydration reaction not having reached completion after 8 hours. This excess heat of hydration resulted in the mortar bar being hotter than the 20^{o}C at the time the test was performed. The shrinkage is therefore a thermal contraction that occurs over the three days while the sample is under water. The required temperature decrease that would result in 150 microstrain shrinkage would be approximately 15^{o}C. This thermal contraction did not occur with the CA cement left in the mold for 24 hrs.

4.3 Summary of Laboratory Test Results

The laboratory test results comparing the Palmdale cement to the standard Type II Portland cement showed shrinkage of the cement was the most likely reason for the observed cracking on the Palmdale test sections. The difference in the coefficient of thermal expansion between the Type II and Palmdale concrete was insignificant. Both the mortar bar and concrete drying shrinkage test indicated that the Palmdale cement had a significantly higher shrinkage as compared to a Type II cement. Although free shrinkage tests do not always directly correlate to field performance, there appears to be enough physical evidence in terms of field cracking, field strain measurements, and laboratory test results that the failure of these test sections were a result of a high shrinkage cement coupled with the environment in Palmdale. To validate these initial findings, concrete pavement analysis needs to be completed to calculate stresses in the concrete due to the environmental effects and measured material properties.

5 CONCRETE PAVEMENT MODELING OF ENVIRONMENTAL EFFECTS

Analysis of axial effects was performed using continuum mechanics while bending stresses were modeled using the ILSL2 (ILLISLAB2) finite element program (Khazanovich, 1994) which is an updated version of the ILLISLAB program developed at the University of Illinois (Tabatabaie-Raissi, 1977).

5.1 Model parameters

5.1.1 Temperature

The thermal shrinkage (axial) from the change in temperature after construction (Figure 3.5 and Table 3.4) and the change in temperature with the change in seasons (Figure 3.6) was modeled using the coefficient of thermal expansion and the average temperature through the slab.

The maximum temperature differential soon after construction was approximately 5.0 ^{o}C which occurred approximately 16:00, two hours after construction (Table 3.4 and Figure 3.5). Paving during the heat of the day can result in residual tensile stresses at the top of the slab. The average slab temperature differential after construction was approximately 6.5 ^{o}C at 16:00. This would result in a slight (6 με) positive bending strain which would be more than offset by the large (250 με) negative bending strain caused by drying shrinkage (see later). This small bending effect from warm weather paving was therefore ignored in the analysis.

The ILSL2 package allows separation between an existing slab and an overlay or

base, which is critical in accurately modeling the stresses in overlays or slabs on stiff bases. In addition to the layer separation, ILSL2 allows non-linear temperature gradients to be used in the analysis, which can significantly affect the maximum stresses at the top of the slab.

One problem with the layer separation model used in ILSL2 is that only a single slab can be modeled. This prevents dowel bars, tie bars and adjacent slabs from being modeled. If no layer separation model is used, adjacent slabs and dowels can be included. A layer separation model was not required for this analysis since the base was a 100 mm lightly cemented layer.

The temperature gradients used in the modeling were the worst case temperature gradients measured in the test sections (Table 3.6 and Figure 3.8). These values are all for 200 mm slabs.

5.1.2 Drying shrinkage

The shrinkage model used assumed more shrinkage at the top of the slab than at the bottom. The data from Palmdale indicated little to no drying shrinkage below the slab mid-depth which is consistent with previous observations (Rasmussen and McCullough, 1998). The shrinkage below the slab mid-depth that is shown in Figure 3.15 was due to thermal effects after construction, as explained previously. The shrinkage model used in the analysis was the bi-linear model from Figure 2.5 as used in the HIPERPAV software (Rasmussen and McCullough, 1998).

The maximum shrinkage differential measured by the Carlson A-8 strain gages was approximately 150 με, as shown in Figure 3.15. This was determined from the

average strains measured 38 mm from either the top or bottom of the 200 mm slabs. As a bi-linear shrinkage distribution was assumed, this value was increased to 250 με through the whole slab. Although there was no data on the shape of the shrinkage gradient, the actual shrinkage distribution is likely to be non-linear.

5.1.3 Slab dimensions

The slab lengths used were 3.7 m, 4.5 m and 6.0 m, which are typical of short, intermediate, and long slabs encountered in the Palmdale test sections. The slab widths were 3.66 m and 4.26 m which are typical for normal and widened lane widths respectively (Figure 3.1).

The slab thickness was 200 mm for the analyses as this is the only test slab thickness for which there was temperature and shrinkage data.

5.1.4 Concrete properties

The concrete slab elastic modulus was taken as either 35 GPa which was assumed as a typical value for concrete pavements or as 50 GPa which could be achieved with high cement contents and fast setting concrete mixes. Back-calculation using falling weight deflectometer (FWD) results at the Palmdale test sections indicated an elastic modulus of approximately 35 GPa (Roesler, et al, 1998).

The average concrete coefficient of thermal expansion from laboratory testing was 8.0 E-06/°C (see Section 4.1). The concrete strengths are given in Section 3.2.2. The average flexural strength after 90 days was 5.14 MPa.

5.1.5 Slab support conditions

A Winkler foundation was used in the analysis with the coefficient of subgrade reaction taken as either 50 MN/m^3 or 150 MN/m^3. The back-calculated k-values decreased after the first day test values, which could be related to slab lift-off or environmental cracking. The average k-value after the first day ranged between 100 to 210 MN/m^3. After 90 days, the average k-value ranged between 75 and 128 MN/m^3. The k-values were back-calculated using the test results from a Dynatest HWD (Roesler, et al, 1998).

5.1.6 Load transfer devices

In all cases, three slabs were analyzed together and the stresses and deflections for the center slab taken. Load transfer was achieved by modeling aggregate interlock or both aggregate interlock and dowels. For the aggregate interlock, a non-dimensional aggregate interlock factor of 10 was used which represents a load transfer efficiency of 80 percent (Ioannides and Korovesis, 1990). The dowels used in the analysis were 384 mm long, 25 mm diameter solid steel dowels with a spacing of 300 mm, placed at the mid-depth of the slab.

5.2 Results

The following is a summary of the model inputs for the analysis purposes. The first value is the value used in the standard analysis case and the values in brackets are the values that were used to determine the sensitivity of the stresses and deflections to the various model parameters.

- Thickness 200 mm
- Length 4.5 m (3.7 m and 6.0 m)
- Width 3.66 m (4.26 m)
- No temperature gradient (Max positive, max negative and max negative for top 50 mm – Table 3.4 and Figure 3.5)
- Shrinkage gradient of 250 με (125 με)
- Coefficient of subgrade reaction of 150 MN/m^3 (50 MN/m^3)
- Concrete modulus of 35 GPa (50 GPa)
- Non-dimensional aggregate interlock factor of 10 (aggregate interlock and dowels)

The stress and deflection distributions for the standard slab assumptions given above are shown in Figure 5.1. The slab stresses and deflections for the other cases are given later in the report. The critical stresses were determined to be at the top of the slab in all cases and as a result, top of slab stresses are shown in the figures. As plate theory was used in the analysis, the deflections at the top and base of the slab are equal. The sign convention is positive deflection downward and tensile stresses are positive.

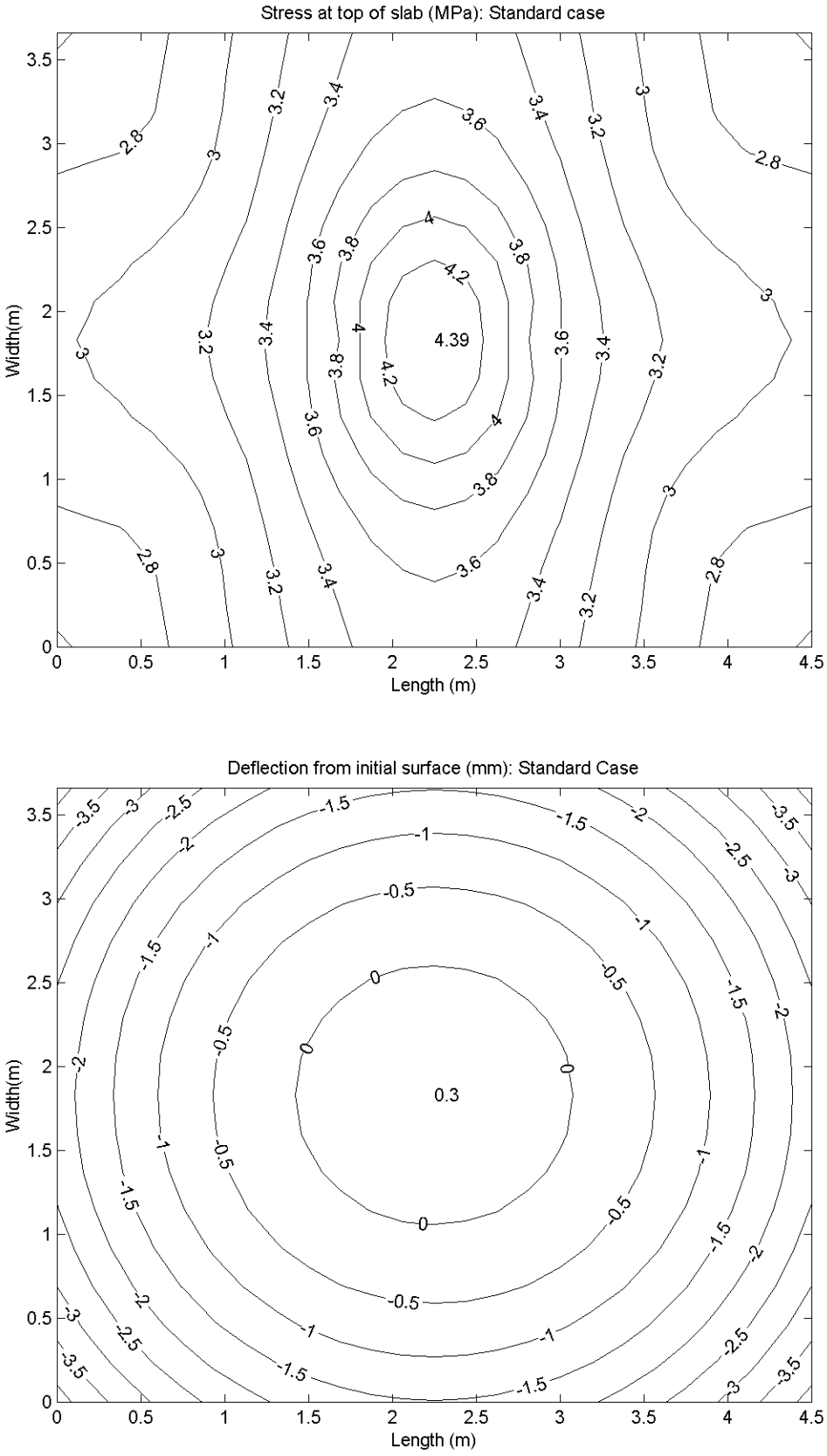

Figure 5.1. Stresses and deflections at top of slab for standard analysis case.

As shown in Figure 5.1, the stress and deflection distributions are symmetrical about the slab centerline. The maximum predicted tensile stress is 4.39 MPa at the center of the slab. This shrinkage-based stress is 85 percent of the flexural strength of the concrete.

The slab has an upward curl resulting from the shrinkage gradient. The corners are approximately 4 mm above the initial position and the center is approximately 0.3 mm below this position. This shrinkage gradient results in the slab corners being in an unsupported condition.

5.2.1 Effect of uniform cooling

The effect of uniform cooling after construction and with seasonal temperature changes was modeled using the following formula:

$$e_t = a \cdot \Delta T$$

The equation parameters are given in Section 2.1. As the average temperature in the slabs decreased from 39^{o}C immediately after construction (Table 3.4) to an average of approximately 25^{o}C during the month of construction (Figure 3.6), the temperature decrease from the heat of hydration of the concrete to ambient temperatures can be assumed to be 14^{o}C. Using the average coefficient of thermal expansion of 8.0E-06 from laboratory testing (Table 4.2) and the temperature decrease, the expected thermal contraction for the unrestrained case would be 112 με. This compares fairly well to the data in Figure 3.14, which indicates contraction of between 100 and 150 με at the base of

the slab in the first few days after construction.

The change in average slab temperature from summer to winter was approximately 25^{o}C (Figure 3.6). This would result in a thermal contraction strain of approximately 200 με. This also correlates well with the measured data in Figure 3.14 where the shrinkage at the base of the slab changed from approximately 100 to 300 με from the middle of summer to the middle of winter.

In both cases, the contraction at the top of the slab is higher than the contraction at the base. This difference can be explained by the drying shrinkage at the top of the slab. The axial thermal shrinkage effects (from cooling) will not cause any stresses in the slab unless there is some restraint to movement. If there is 100 percent restraint then no measurable strain will result. In this fully restrained case, the internal stress in the slab will be the predicted free strain times the concrete modulus. Since it is difficult to determine the amount of restraint, this analysis does not include the effects of the axial thermal contraction or drying shrinkage. Since the calculated free strain based on the pavement temperatures over the seasons and due to heat of hydration were close to the measured strains in slab, it can be assumed that very little axial restraint existed due to uniform temperature changes.

5.2.2 Effect of temperature gradient

The effect of the temperature gradient on the slab stresses and deflections is illustrated in Figures 5.2 to 5.4. The temperature gradients used are those illustrated in Figure 3.8.

It is important to note that the maximum shrinkage differential through the slab (used in the standard case analysis) and the maximum temperature gradients did not necessarily occur at the same time and the combined analysis may therefore slightly over-predict the slab stresses.

As can be seen in Figure 5.2, the maximum tensile stress (3.43 MPa) and corner deflection (1.2 mm) under the maximum positive temperature gradient and average shrinkage gradient are approximately 22 and 70 percent lower than for the shrinkage gradient only case (Figure 5.1). This is because a positive temperature gradient has the opposite effect to the shrinkage gradient through the slab.

Figure 5.3 illustrates the combined effect of the maximum negative temperature gradient through the slab and the shrinkage gradient. The maximum tensile stress (4.89 MPa) and corner deflection (5.7 mm) are approximately 11 and 36 percent higher than for the standard case as the negative temperature gradient adds to the shrinkage gradient through the slab.

The temperature gradient that results in the highest tensile stresses was the maximum negative gradient for the top 50 mm (Figure 3.7). The maximum tensile stress (5.62 MPa) and corner deflection (5.3 mm) are 128 and 127 percent of the shrinkage gradient only case. The stresses for this case are 15 percent higher than for the maximum negative temperature gradient, but the deflections are 7 percent lower. This is because of the non-linear nature of the temperature distribution increases the axial stresses which won't have an effect on the slab deflections.

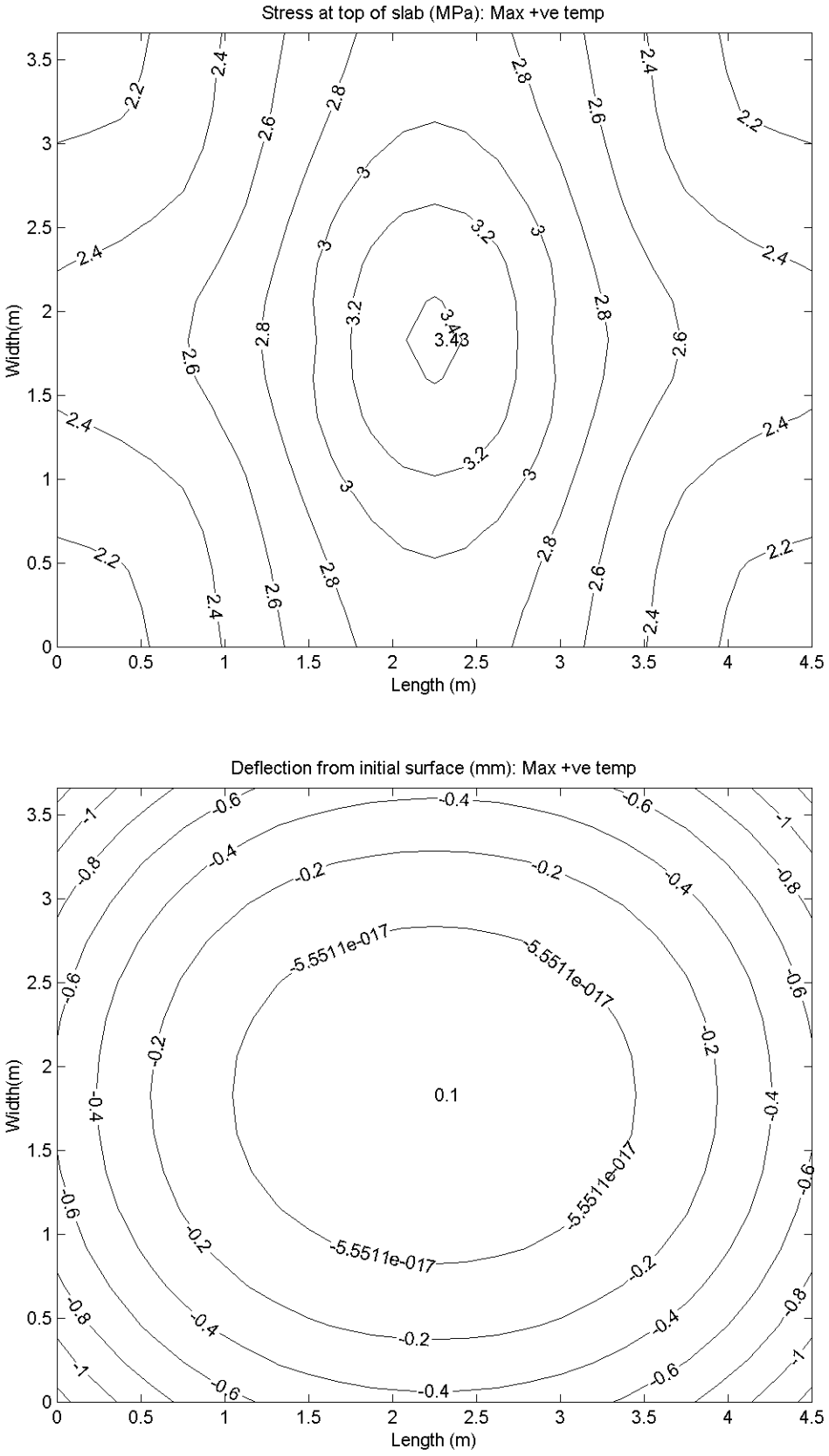

Figure 5.2. Stresses and deflections under maximum positive temp gradient

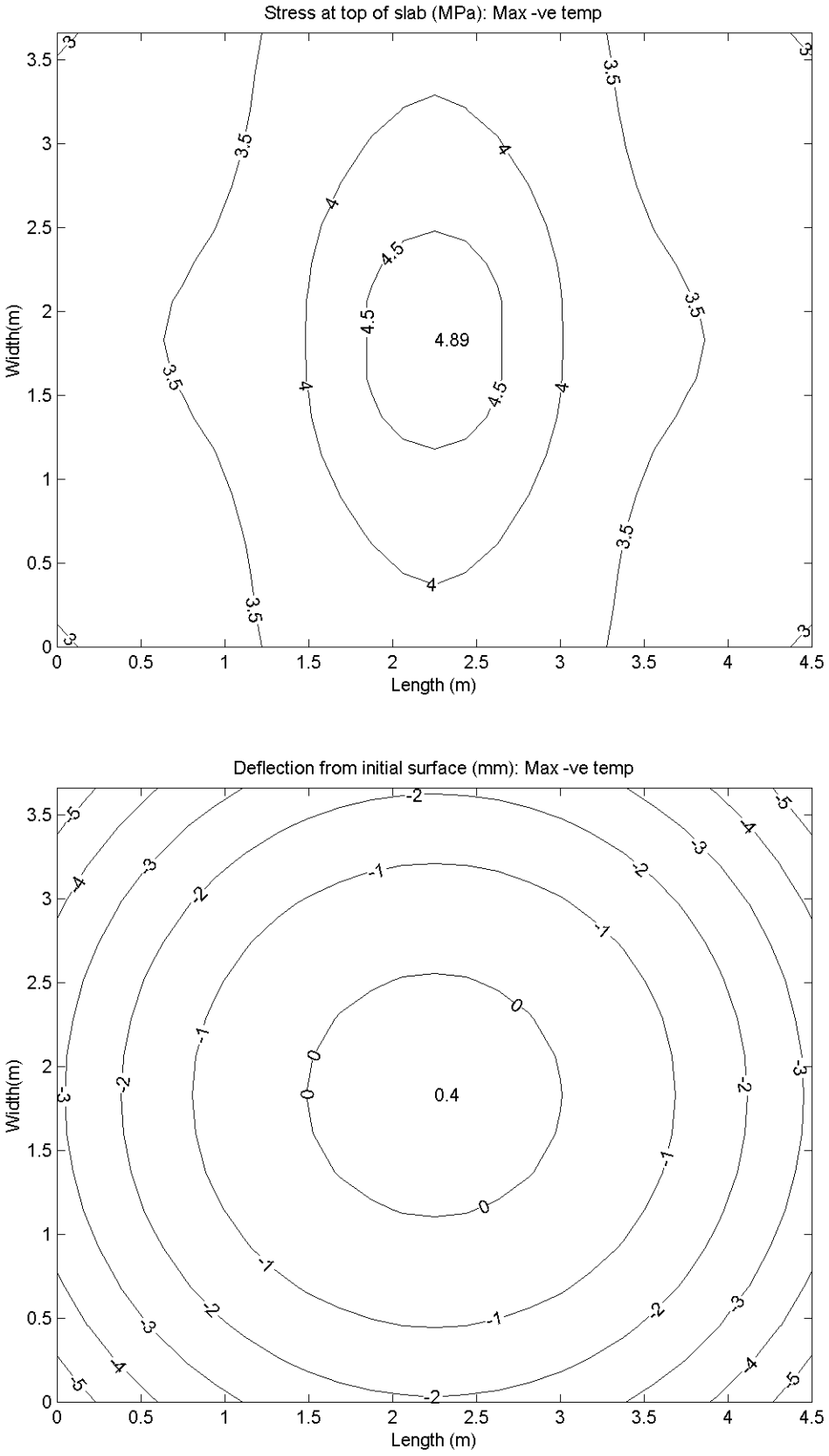

Figure 5.3. Stresses and deflections under max negative slab temp gradient

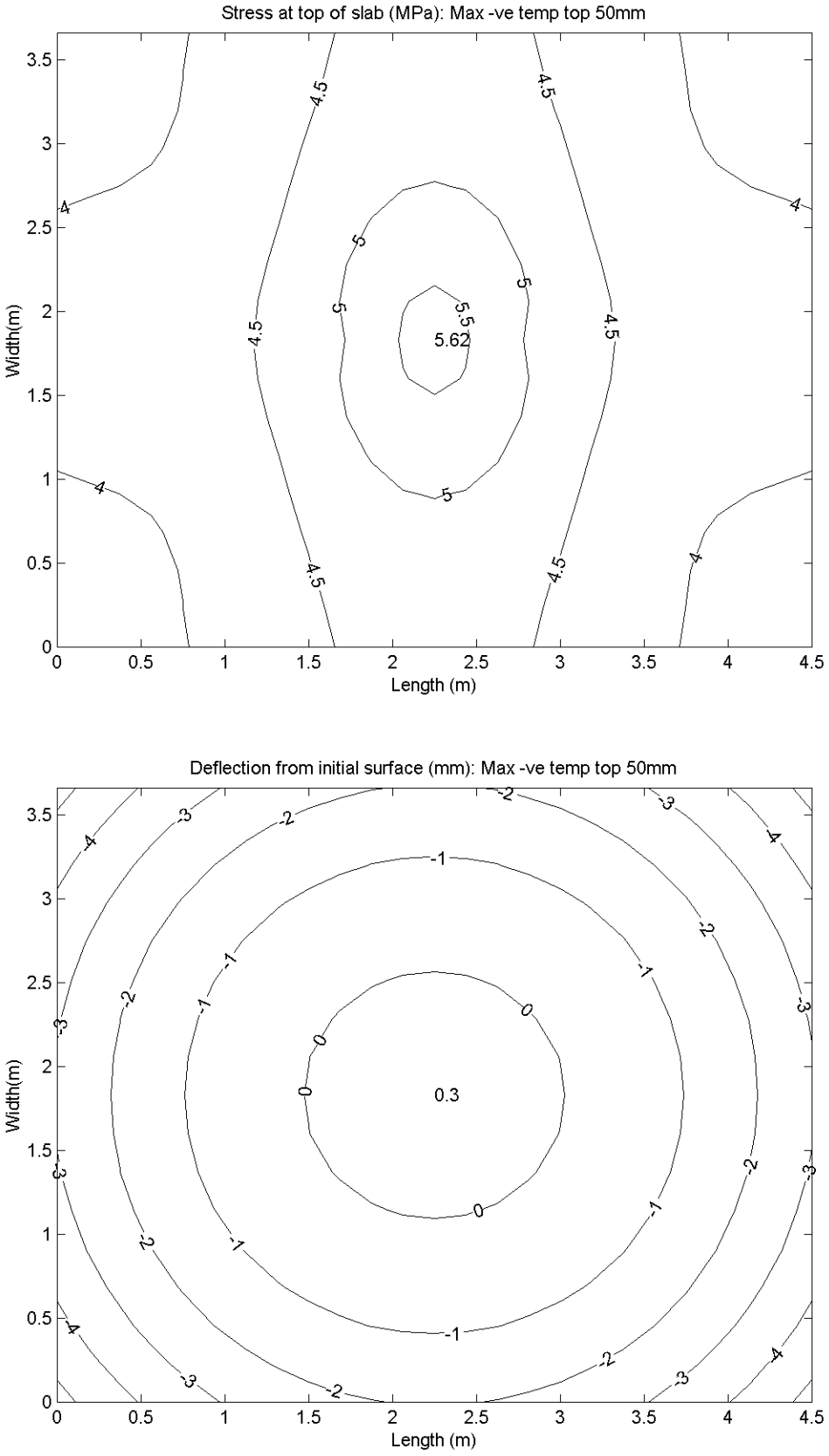

Figure 5.4. Stresses and deflections under max negative top 50mm temp gradient

5.2.3 Effect of shrinkage gradient

The shrinkage gradient through the slab was reduced to 125 με in the analysis to determine the effect on environmental stresses. The standard case had a shrinkage gradient of 250 με, which was the differential measured at the Palmdale test sections. In both cases a bi-linear shrinkage model (Figure 2.5) was used where no shrinkage was assumed below the mid-depth of the slab. The stresses and deflections under the 125 με shrinkage gradient are illustrated in Figure 5.5. As shown, the stresses for the slab with the lower shrinkage gradient were reduced to 64 percent of those under the shrinkage gradient of 250 με. Analysis with no shrinkage or thermal gradient results in no slab stresses or deflections.

As the cement used in the construction of the Palmdale test sections had one of the highest free shrinkage values of all the different cement types tested (see Section 4.2), the lower shrinkage analysis may be a realistic scenario for pavements constructed using other fast setting hydraulic cements. The residual shrinkage gradient for most concrete slabs is probably less than 125 με. More field shrinkage measurements are required for other cement types, both FSHCC and PCC.

Concrete pavements constructed with conventional cements (e.g. Type II Portland cement) may have stress relaxation as the strength and elastic modulus increase is slower for PCC than for FSHCC. This would lead to the combined differential shrinkage and creep effect resulting in low differential strains and therefore low environmental stresses. This could result in the maximum environmental stress moving to the bottom of the slab, resulting in bottom up cracking under positive temperature gradients.

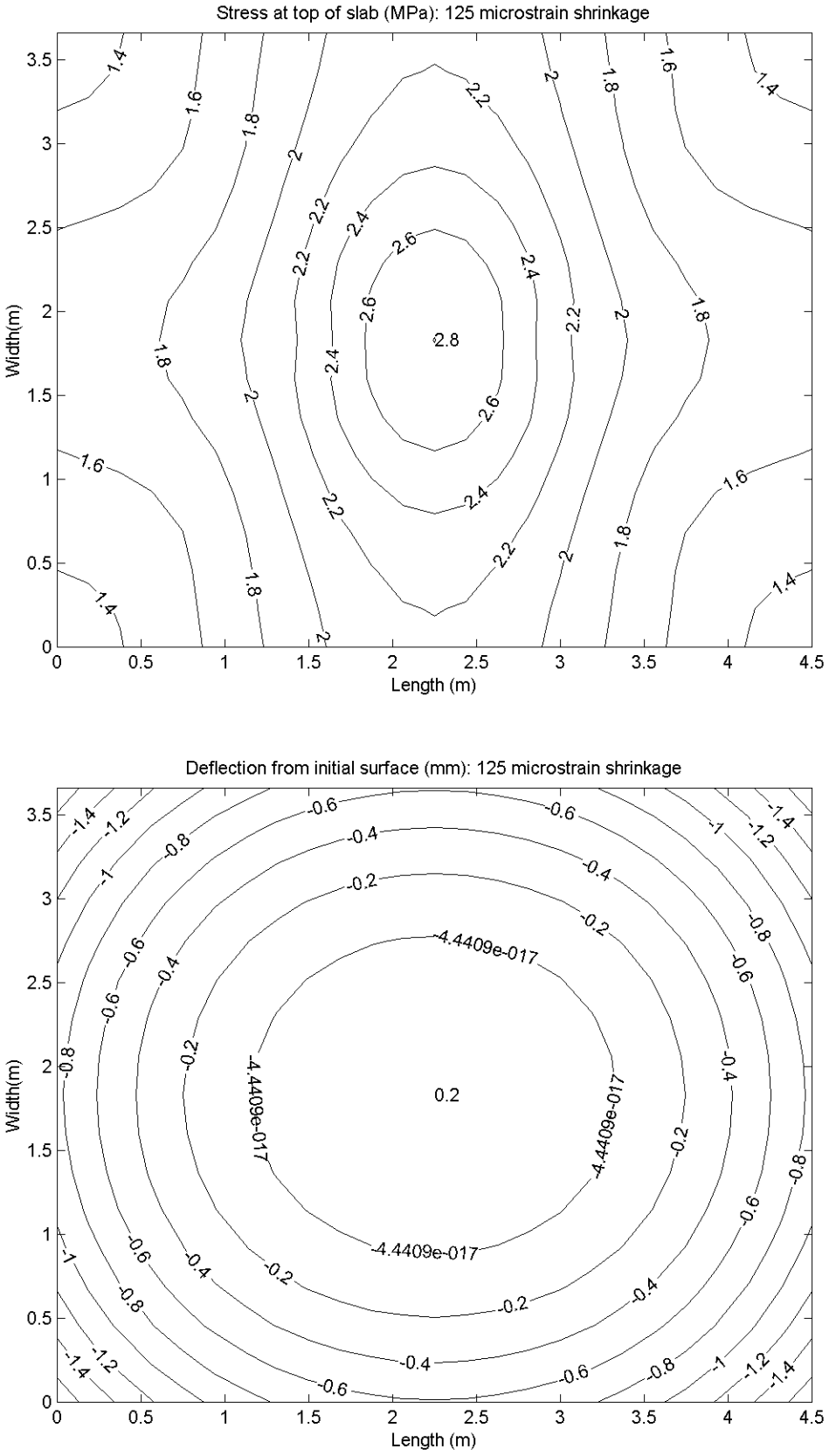

Figure 5.5. Stresses and deflections under 125 με (low) shrinkage gradient

5.2.4 Effect of slab length

The effect of slab length on the shrinkage-induced stresses was determined by analyzing slab lengths of 3.7 m (short slab), 4.5 m (standard case) and 6.0 m (long slab) under the standard 250 με shrinkage gradient. These represent short, medium and long slabs at the Palmdale test sections.

The results of the analysis with different slab lengths can be seen in Figures 5.6 and 5.7 for the long and short slabs, respectively. The stress and deflection distributions for the 4.5 m long slab (standard case) are shown in Figure 5.1.

As shown in the figures, the maximum tensile stress for the long, medium and short length slabs are 5.54, 4.39 and 3.88 MPa, respectively. The average concrete strength 90 days after construction (when the maximum shrinkage differential was noted) was 5.14 MPa. This explains why all the longer slabs at Palmdale (5.5 to 6.0m) cracked under environmental influences and the shorter slabs (< 4.0 m) did not experience environmental cracking.

The combined effect of negative temperature differentials and the slab shrinkage will increase these stresses even further.

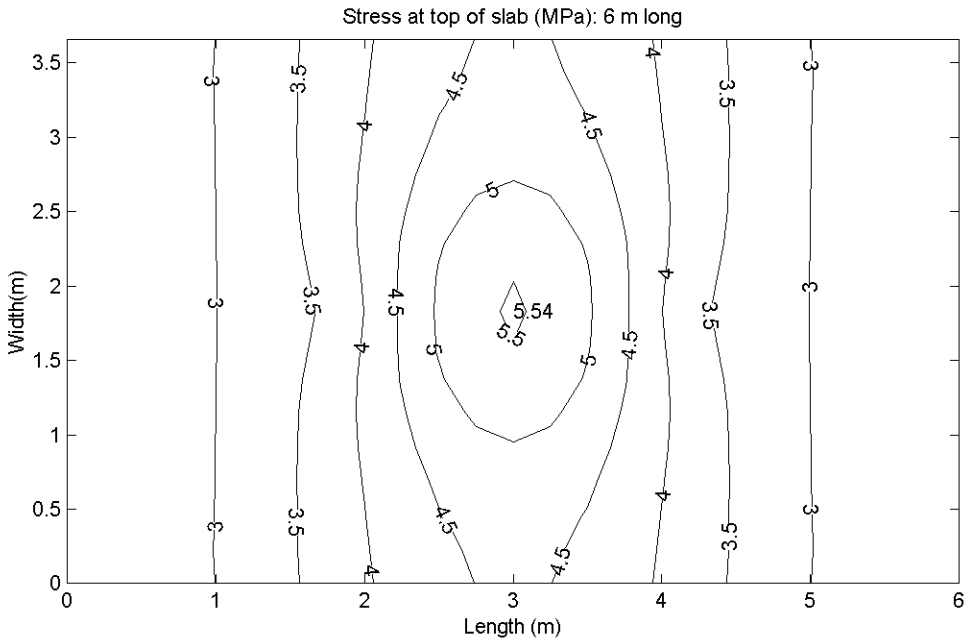

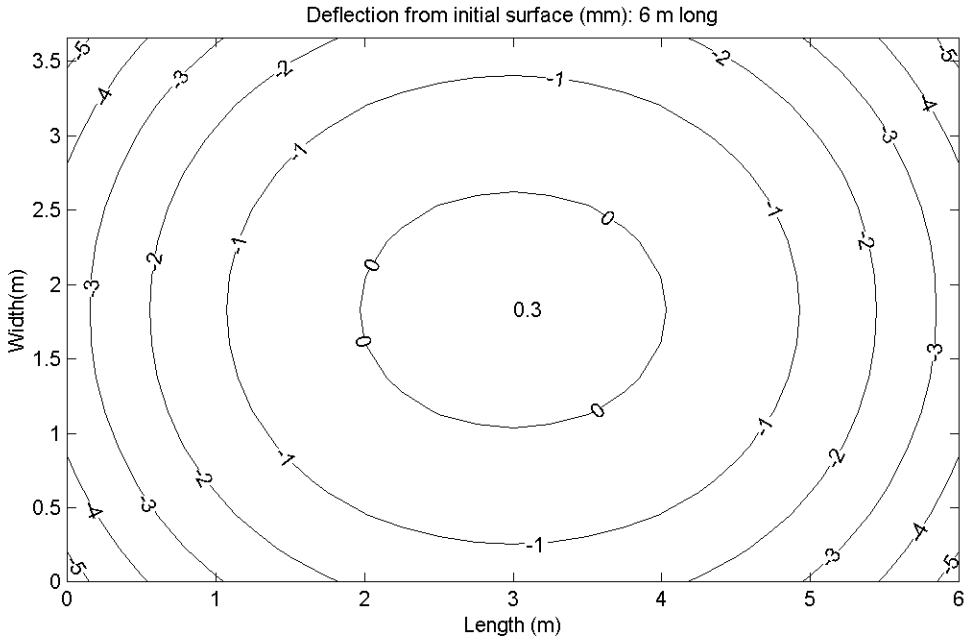

Figure 5.6. Stresses and deflections for 6.0 m (long) slab

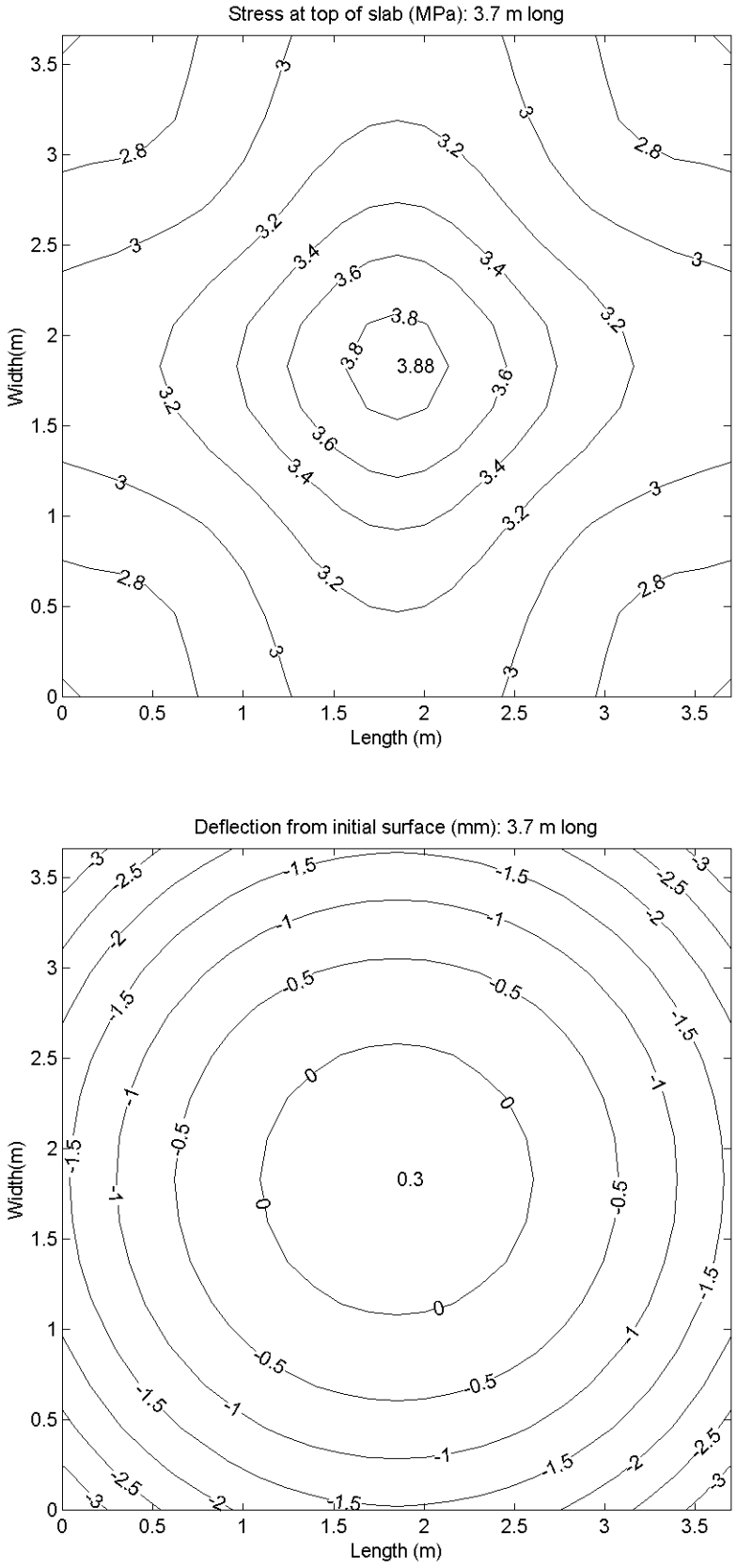

Figure 5.7. Stresses and deflections for 3.7 m (short) slab

5.2.5 Effect of slab width

The effect of slab width on stresses and deflections was determined by comparing a 4.26 m wide slab with a 3.7 m wide slab, both subjected to a 250 με shrinkage differential. The wider slab is proposed for widened truck lanes to prevent heavy vehicles from driving on the outer slab edge.

The stresses and deflection for the 4.26 m wide slab are illustrated in Figure 5.8. The maximum stress of 4.53 MPa is only 3 percent higher than a 3.66 width slab (Figure 5.1). The corner deflection of 4.75 mm is 13 percent higher than the standard width.

5.2.6 Effect of slab stiffness

The effect of slab stiffness on the shrinkage stresses was determined by analyzing a slab with the concrete elastic modulus increased from 35 GPa to 50 GPa. The results of the analysis are shown in Figure 5.9 and can be compared to Figure 5.1.

The maximum stress and corner deflection for the increased modulus case were 5.53 MPa and 4.41 mm, 26 and 5 percent higher than the standard case, respectively. While an increased modulus can decrease stresses and deflections for slabs undergoing traffic loading, the higher modulus increases stresses for environmental loading. This is because the environmental loading results in strain, which is largely independent of the slab elastic modulus. As the stress is equal to the strain times the elastic modulus, the resulting stress increases with increasing modulus.

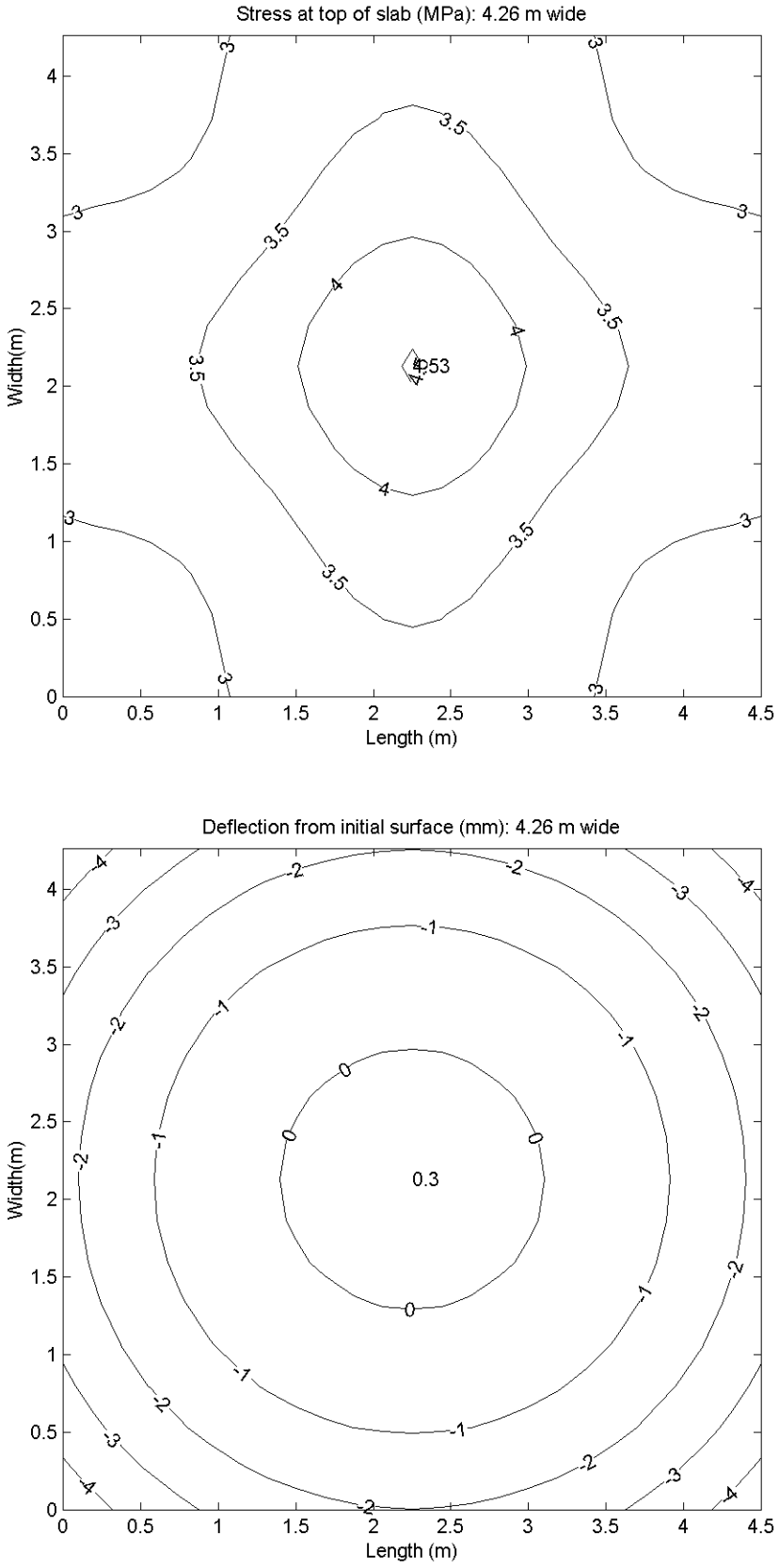

Figure 5.8. Stresses and deflections for 4.36 m (wide) slab

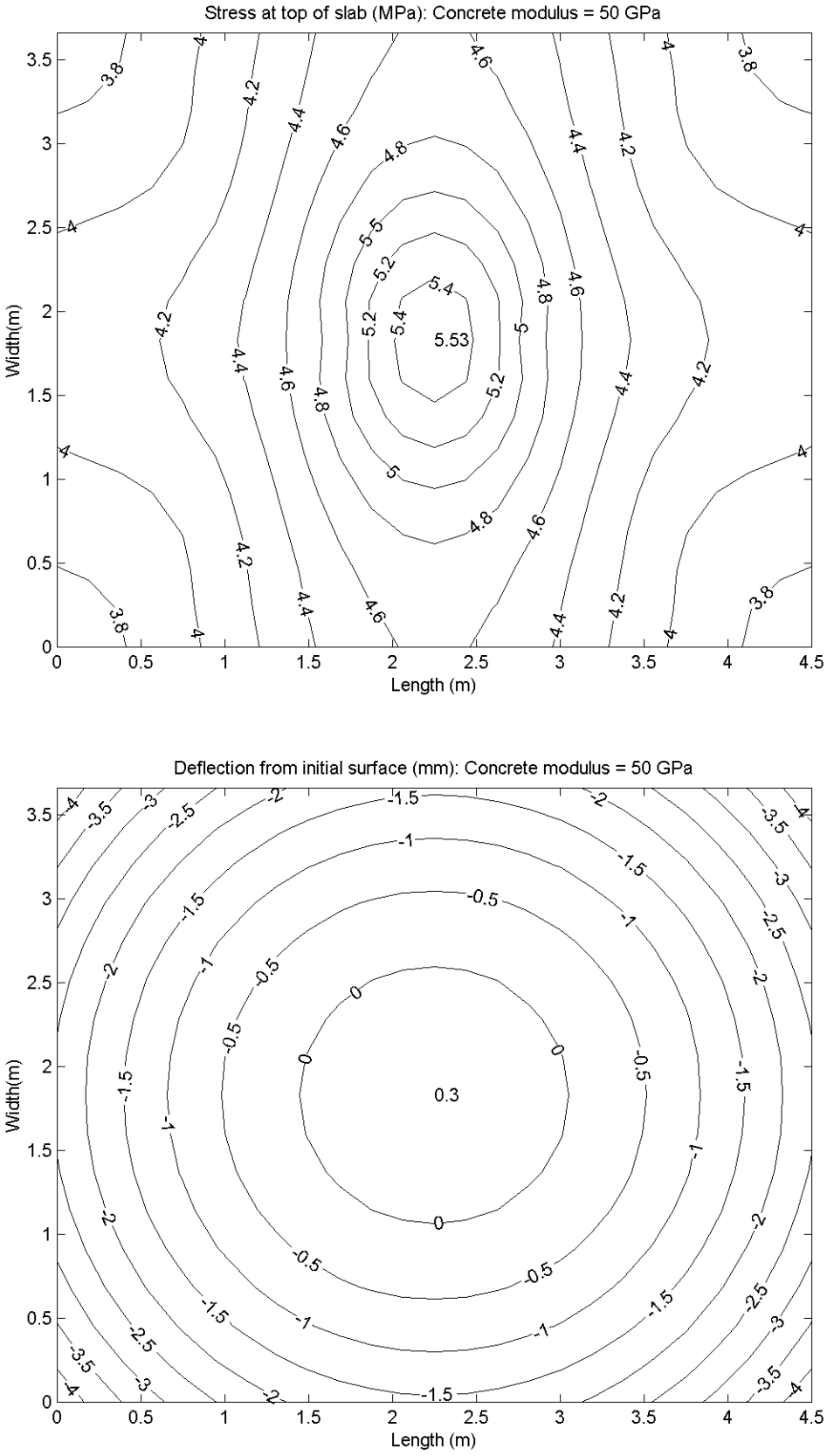

Figure 5.9. Stresses and deflections for 50 GPa (high) modulus concrete

5.2.7 Effect of subgrade support

The effect of subgrade support on the shrinkage stresses was determined by decreasing the coefficient of subgrade reaction from the value of 150 MN/m^3 used for the standard case to 50 MN/m^3. The stress and deflection distributions for this case are shown in Figure 5.10. The maximum stress and corner deflections are 3.96 MPa and 3.9 mm, reduced 10 and 8 percent from the standard case, respectively. The reduction in stresses with a lower k-value is a result of the support uniformly accommodating the curled slab.

While a lower coefficient of subgrade reaction can reduce the environmental stresses, it does increase the stresses under traffic loading. The magnitude of the stress increase depends on the load location and whether the slab is fully supported. It is important to have uniform support under the slab in order to reduce stresses. One way of achieving all of these is to have a subgrade that can relax under long-term loading but is stiff under rapid loading. An example of this is a rich asphalt concrete mix.

5.2.8 Effect of load transfer devices

The stresses and deflections for a slab with 25mm dowels as load transfer devices between adjacent longitudinal slabs instead of aggregate interlock is illustrated in Figure 5.11. The maximum stress and corner deflection for this case were 5.28 MPa and 3.61 mm. These are 120 and 86 percent of the standard case, respectively. While the installation of load transfer devices may increase environmental stresses, dowels decrease stresses under traffic loading, particularly for the unsupported corner load situation.

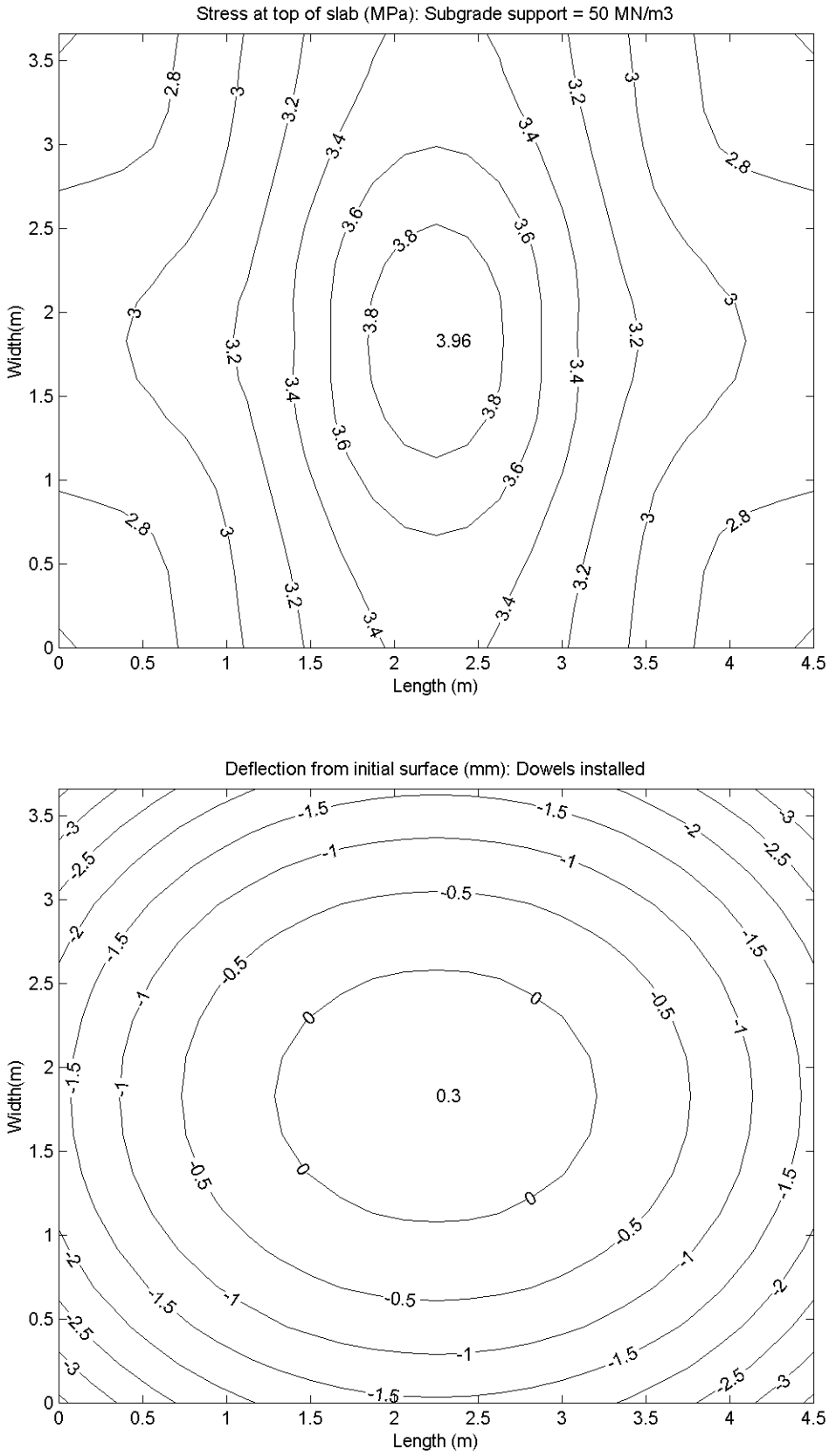

Figure 5.10. Stresses and deflections for 50 MPa/m (low) k-value

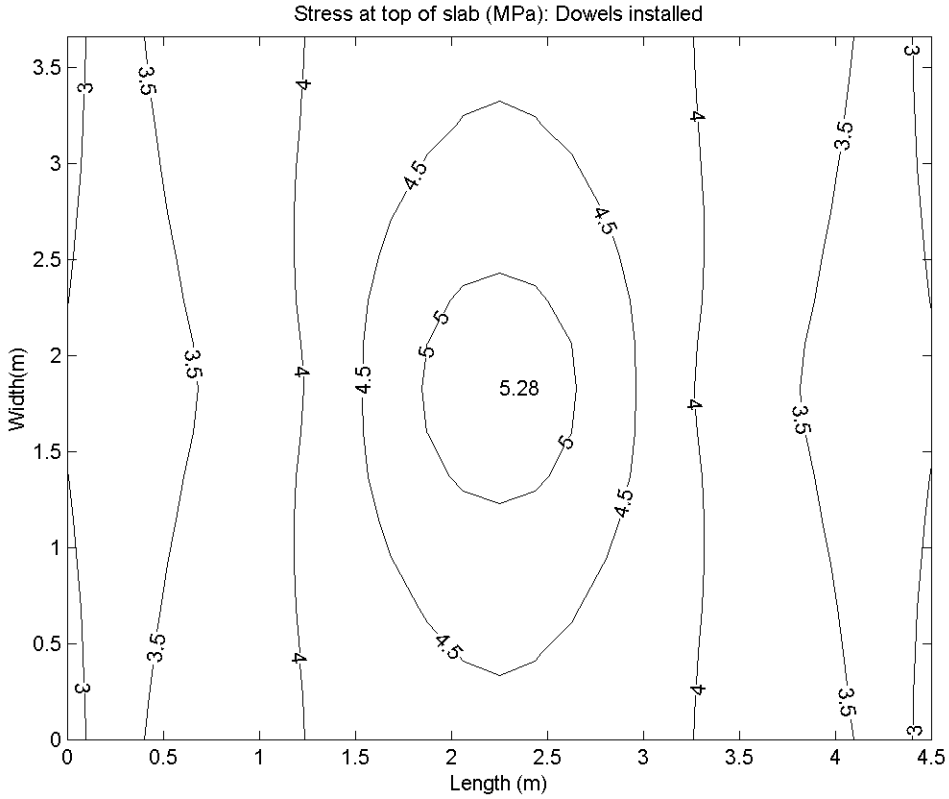

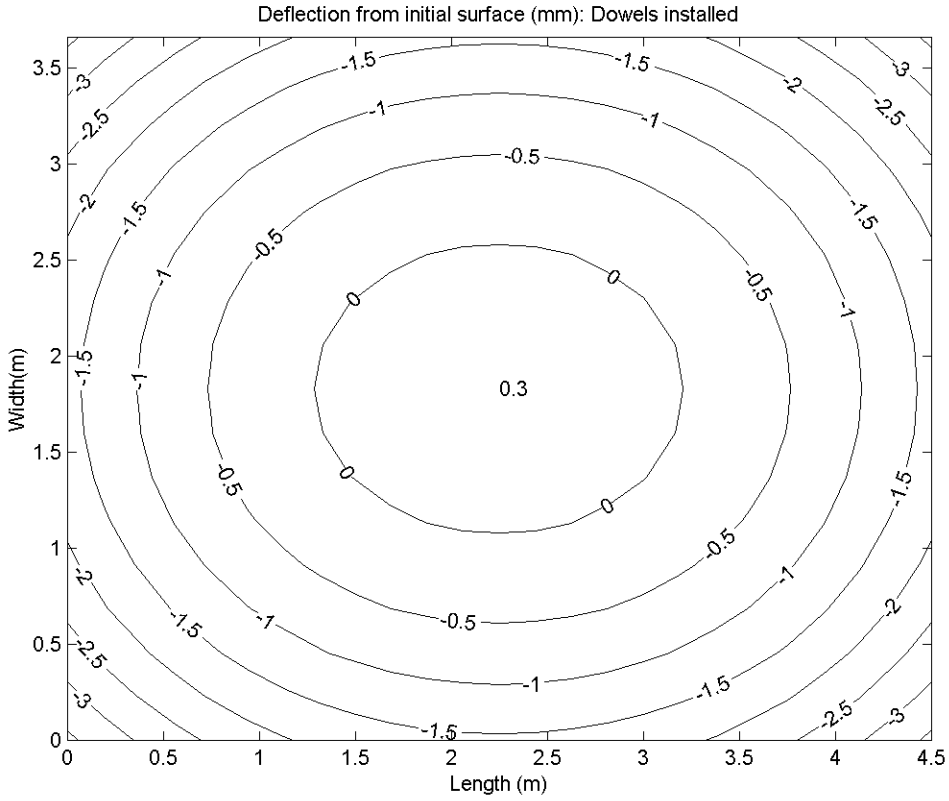

Figure 5.11. Stresses and deflections for concrete slab with dowels

5.3 Analysis and summary

5.3.1 Validation of finite element model

The results from the finite element analysis were validated by comparing the calculated deflections with the measured deflections. The measured strains were used as inputs to the finite element program to reproduce the shrinkage gradient observed in the field slabs. The predicted tensile bending stresses for the longer slabs were above the flexural strength of the concrete, while the stresses for the shorter slabs were not. Field surveys found only environmental cracking on the longer slabs (5.5 to 6m).

The predicted and measured corner deflections during a typical daily temperature cycle are illustrated in Figure 5.12. The deflections are for a 3.66 m x 3.96 m x 200 mm slab. This slab size was chosen since the deflection measuring devices (JDMDs) were located on these slab and they were not cracked. Included in the figure are deflection predictions for a 250 με shrinkage gradient through the slab (measured in Palmdale) and for no shrinkage gradient (often assumed in rigid pavement analysis). The average measured concrete coefficient of thermal expansion of $8.0 \times 10^{-6}/°C$ was used in the analysis. Figure 5.12 shows a permanent upward curl in the slab had to exist to match the measured deflections in the field to the finite element results. Without a residual shrinkage gradient in the slab, the finite element analysis under predicts the corner deflection by a factor of 3 for most of the day. By matching the measured and calculated corner deflections, it can be confidentially assumed the slab corner and edges are unsupported most of the time and the calculated stresses are reasonable.

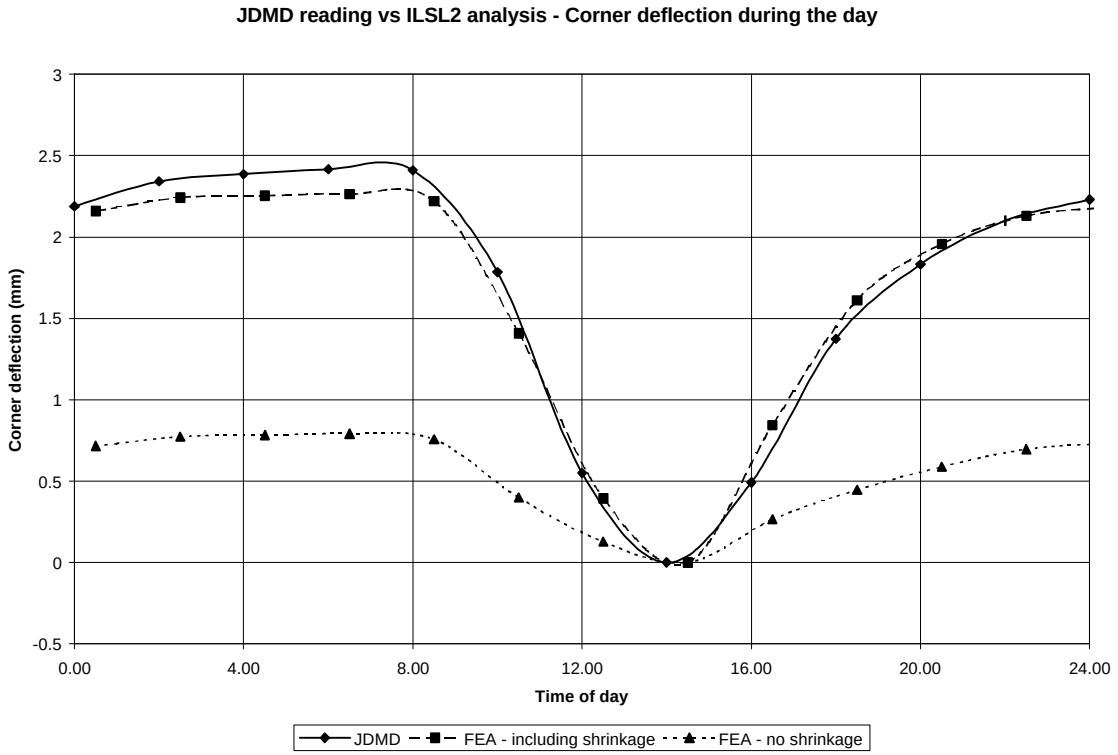

Figure 5.12. Measured and predicted corner deflections during a daily cycle.

The calculated deflections had to be adjusted by approximately 30 minutes to match the measured deflections. This could be because the slab takes a finite time to reach equilibrium given a certain temperature profile, especially when the temperature profile is changing more rapidly during the middle of the day.

The measured and calculated corner deflections in Figure 5.12 were plotted versus the measured temperature gradient in the slab for a day, as shown in Figure 5.13. The measured data is the same as in Figure 3.13. For this analysis, the temperature gradients were shifted by 30 minutes for the calculated deflections, as described above. Again, the measured and calculated deflections match each other when the shrinkage gradient in the concrete slab is considered. If the shrinkage gradient is ignored, then the corner

deflections are significantly lower than the measured deflections. Field measured deflections can be misinterpreted without consideration of the residual stresses in the concrete slab.

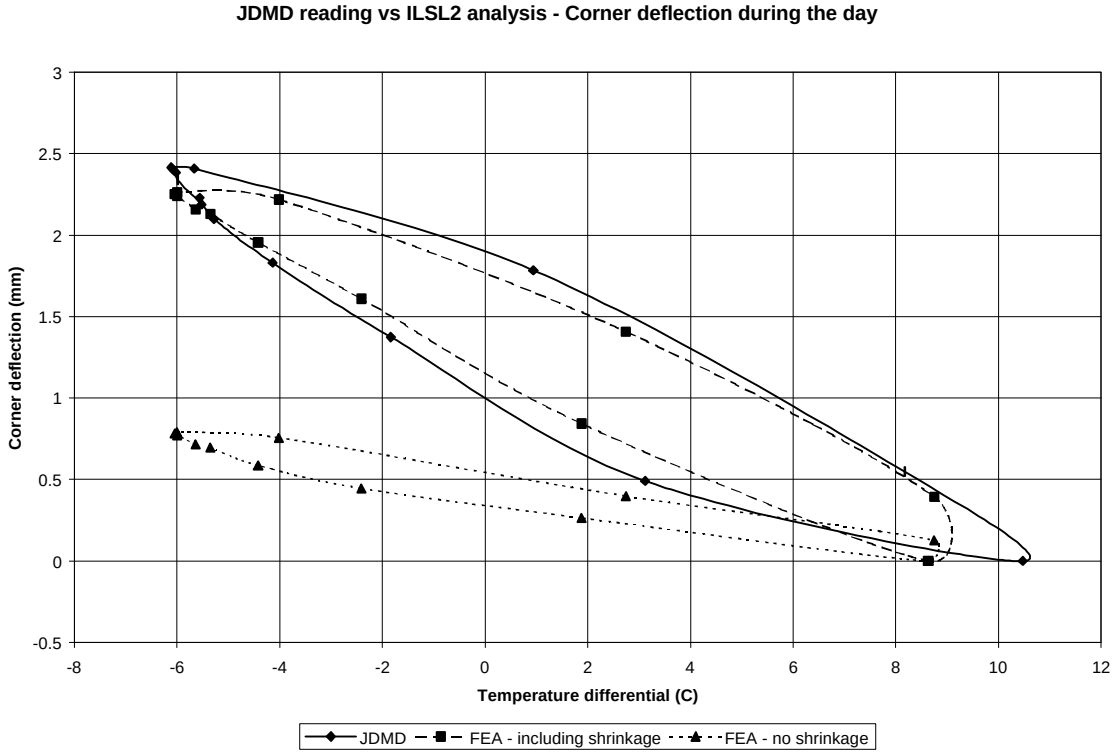

Figure 5.13. Measured and predicted corner deflections vs temperature gradient

5.3.2 Summary of findings

A summary of the stresses and deflections obtained for the different cases investigated are given in Table 5.1. Included in the table is the percent of standard case for each of maximum tensile stress, center deflection and corner deflection.

Table 5.1. Summary of stresses and deflections for environmental loading cases

Load case	Max tensile stress		Center deflection		Corner deflection	
	MPa	% std	mm	% std	mm	% std
Standard (no temperature gradient)	4.39	100	0.30	100	-4.2	100
Max +ve temp gradient	3.43	78	0.15	50	-1.27	30
Max –ve slab temp gradient	4.89	111	0.35	119	-5.73	136
Max –ve top 50 mm temp gradient	5.62	128	0.34	115	-5.33	127
Shrinkage = 125 με (low shrinkage)	2.80	64	0.18	61	-1.74	41
Length = 6.0 m (long slab)	5.54	126	0.30	103	-5.42	129
Length = 3.7 m (short slab)	3.88	88	0.28	95	-3.49	83
Width = 4.26 m (wide)	4.53	103	0.31	104	-4.75	113
Slab E = 50 GPa (stiff)	5.53	126	0.31	106	-4.41	105
Subgrade K = 50 MN/m3 (soft)	3.96	90	0.70	236	-3.89	92
Dowels installed	5.28	120	0.28	96	-3.61	86

As shown in the table, the most critical factors influencing the environmental tensile stresses are the temperature gradient, magnitude of shrinkage differential, slab length, slab modulus and the installation of dowels.

Of the above factors, the temperature gradient is most difficult to control. The use of aggregates with a low coefficient of thermal expansion will be impractical and probably expensive in most situations.

The slab length is the easiest to control of all the factors. It is important to use joint spacing of four to five times the radius of relative stiffness. This will dramatically decrease the magnitude of the environmental stresses especially if excessive shrinkage

stresses are induced.

The use of low shrinkage cements and proper curing will reduce the stresses in rigid pavement slabs. The fast setting hydraulic cement used in the Palmdale sections had a high shrinkage, which resulted in environmental cracking of the long slabs. However, the experimental results in Section 4 showed some fast setting cements had significantly lower shrinkage than ordinary Portland cement.

While a lower slab modulus will result in lower environmental stresses, it is difficult to achieve this without decreasing the cement content and concrete strength. Decreasing the concrete strength would decrease the pavement life.

While the installation of dowels will increase the environmental stresses in the pavement, additional analysis has shown that the installation of dowels dramatically decreases the stresses under traffic loading, particularly when there is a small shrinkage gradient (<150 με) through the slab.

6 CONCLUSIONS

The transverse cracking of Jointed Plain Concrete Pavement (JPCP) test slabs under environmental loading was investigated. The test slabs were constructed with Fast Setting Hydraulic Cement Concrete (FSHCC) in Palmdale, California as part of the Caltrans accelerated pavement testing program (CAL/APT). Cores drilled above the transverse cracking indicated top-down cracking had occurred.

The shrinkage and thermal properties of in-situ concrete pavements were monitored with strain gages, multi-depth thermocouples, and Joint Displacement Measuring Devices (JDMDs). Initial strains in the slab were most likely due to thermal contraction of the concrete after construction. After two months, strains at the top of the slabs had increased significantly while the strains measured in the bottom of the slab remained constant. It was determined that this increase in the top of slab was a result of drying shrinkage, not thermal contraction. The differential strains through the slab thickness from the combined effect of drying shrinkage and night time temperature gradients resulted in bending stresses, which exceeded the concrete strength and caused transverse cracking. Laboratory testing performed on the cement (calcium sulfoaluminate) and concrete used in the Palmdale test sections showed significantly higher free shrinkage relative to ordinary Type II Portland cement and reinforced the findings of the strain measurements.

JDMDs showed significant corner curling of the field concrete slabs, with as much as 2.5 mm daily movement under environmental conditions. The corner deflection data suggested the slab corners were permanently curled upward caused by the

differential drying shrinkage in the slab.

An analysis of the slab corner deflections was performed by comparing the measured to predicted values from finite element analyses (ILSL2) using non-linear slab temperature profiles and drying shrinkage differentials. The corner deflections under daily temperature cycles were accurately modeled provided the drying shrinkage differential was included in the analysis. The measured data and FEA showed differential drying shrinkage had resulted in the corners of the slab being in a permanently curled up position, resulting in an unsupported corner condition at all times.

By analyzing the differential shrinkage and a negative temperature distribution, the highest tensile stresses from environmental loading were found to be at the middle of the slab at the surface. This validated the field findings that crack initiation began at the top of the slab and propagated downward.

The use of FSHCC does not necessarily indicate high shrinkage differentials as laboratory testing indicated some CS̄A cements can have lower shrinkage than Type II cements.

7 RECOMMENDATIONS

The recommendations in this section are focussed on the use of fast setting hydraulic cement concrete (FSHCC) in rigid pavement rehabilitation. As a result many of the recommendations may not be applicable to Portland cement concrete (PCC) pavements and may be contrary to previous experience with rigid pavements constructed using PCC.

While the testing performed as part of this project did not quantify all aspects of rigid pavement performance under environmental loading, field performance data is available from the Palmdale test sections which enabled model parameters to be accurately determined for that situation. Additional work will be required to determine the thermal expansion and shrinkage parameters for different hydraulic cement concrete mixes under field conditions. Predicting the drying shrinkage gradient through a field slab is the most difficult factor to quantify as this is influenced by creep, elastic deformations and environmental conditions.

The following recommendations will help to increase the life of rigid pavements constructed using FSHCC:

- The shrinkage specification in the project special provisions appears reasonable (0.053% after seven days, according to CTM 527). Shrinkage testing should be performed on the cement proposed for the construction of FSHCC pavements, not only at the beginning of a project, but during the construction in order to check variability in supply.

- Curing conditions have a significant effect on shrinkage and proper curing should always be performed. Alternatives such as double curing membranes should be investigated.

- Bases with a high frictional resistance (e.g. lean concrete bases or open graded mixes) should not be used without a bond-breaking layer between the base and slab. The high frictional resistance can create significant tensile stresses in pavement slabs when the concrete cools from a high heat of hydration (typical with FSHCC) or when the concrete has a high drying shrinkage.

- Flexible bases (for example asphalt concrete mixes) are preferred as they will deform under long-term environmental loading and thereby decrease stresses in the slabs. Stiffer bases (for example lean concrete bases) will not allow any relaxation of environmental stresses.

- Shorter joint spacing (less than 4.5 m) will decrease environmental and traffic load stresses, especially when high shrinkage concrete is used.

- If a long slab replacement is required, placing a doweled joint in the center or placing steel reinforcement to hold cracks together in the slab can increase slab life. Slab replacement is considered a temporary solution.

- New slabs should be prevented from bonding to adjacent slabs as this will induce tensile stresses in the new slab as it shrinks after construction. The joints between the new and adjacent lane slabs must be either cut and

sealed immediately after construction or have a bond-breaker placed between them.

- The time of day and environmental condition when paving is performed should be considered. It is usually preferable to pave under cool, moist conditions and not during the heat of the day.

8 REFERENCES

1. Bradbury, R D. 1938. *Reinforced Concrete Pavements.* Wire Reinforcement Institute, Washington, DC.

2. Farrington, E W, Burns, N H and Carrasquillo, R L. 1996. *Creep and Shrinkage of High Performance Concrete*. Research report 580-5, Center for Transportation Research, University of Texas at Austin, Austin, Texas.

3. Ioannides, A M and Korovesis, G T. 1990. Aggregate Interlock: A Pure Shear Load Transfer Mechanism. *Transportation Research Record 1286, Design and Evaluation of Rigid Pavements*. Transportation Research Board, Washington, DC.

4. Khazanovich, L. 1994. *Structural Analysis of Multi-Layered Concrete Pavement Systems.* Ph.D. thesis, University of Illinois at Urbana-Champaign, Urbana, Illinois.

5. McCullough, D F and Dossey, T. 1999. Considerations for High Performance Concrete Paving : Recommendations from 20 Years of Field Experience in Texas. *Proc. Transportation Research Board Annual Meeting*. Washington, D.C. January 1999.

6. Mohamed, A R and Hansen, W. 1997. *Effect of Nonlinear Temperature Gradient on Curling Stress in Concrete Pavements*. Transportation Research Record No. 1568, Transportation Research Board, Washington, D.C.

7. Meyers, S. L. 1951, *How Temperature and Moisture Changes May Affect the*

Durability of Concrete. Rock Products, pp. 153-57.

8. PCA. *Methods For Reducing Friction Between Concrete Slabs and Cement-Treated Subbases*. Unpublished report by the Cement and Concrete research Institute (a division of the Portland Cement Association) for the Federal Highway Administration, September 1971.

9. Rasmussen, R O and McCullough, B F. 1998. *A Foundation for High Performance Jointed Concrete Pavement Design and Construction Guidelines.* Transtec consultants, Austin, Texas.

10. Roesler, J R; Scheffy, C W; Ali, A and Bush, D. 1998. *Construction, Instrumentation, and testing of Fast-Setting Hydraulic Cement Concrete in Palmdale, California.* University of California at Berkeley, Berkeley, California.

11. Ruth, BE et al, 1993. *Effect of Admixtures and Curing on Shrinkage of Portland Cement Concrete*. University of Florida, Gainesville, Florida.

12. Sargand, S. 1999. *Measurement of Dowel Bar Response in Rigid Pavement*. Ohio Research Institute for Transportation and the Environment, Ohio University, Athens, Ohio.

13. Tabatabaie-Raissi, A M. 1977. *Structural Analysis of Concrete Pavement Joints*. PhD Thesis, University of Illinois, Urbana-Champaign, Illinois.

14. Tia ,M; Bloomquist ,D; Alungbe, G D and Richardson, D. 1991. *Coefficient of Thermal Expansion of Concrete used in Florida.* Department of Civil

Engineering, University of Florida, Gainsville.

15. Wesevich, J W; McCullough, B F and Burns, N H. 1987. *Stabilized Subbase Friction Study for Concrete Pavements*. Research Report 459-1, Center for Transportation research, University of Texas at Austin.

16. Westergaard, H M. 1927. Analysis of stresses in Concrete Pavements Due to Variations of Temperature. *Proceedings: Sixth Annual Meeting, Highway Research Board.* Washington, DC.

17. Wimsatt, A W; McCullough, B F and Burns, N H. 1987. *Methods of Analyzing and Influencing Frictional Effects of Subbases.* Research Report 459-2F, Center for Transpiration Research, University of Texas, Austin.

Appendix A : Environmental crack locations

The cracks indicated are those that were considered to be early age cracks (cracked in the first four months after construction). For slab thickness and joint load transfer devices for the different sections, see Figure 3.1.

Section 11-A, North Tangent
Plan View of Test Area

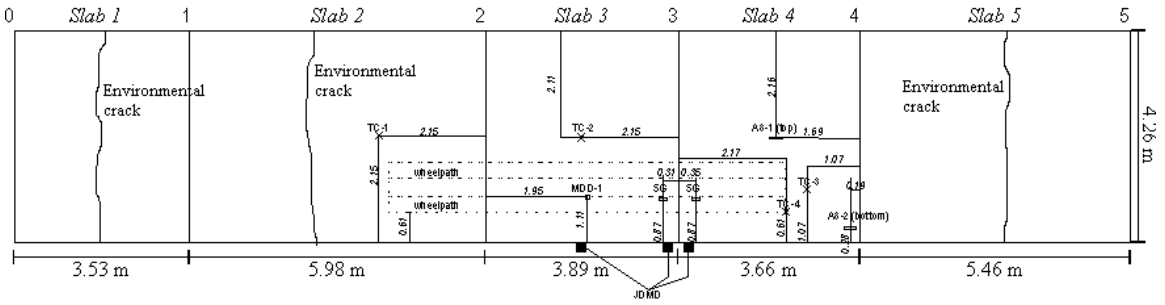

Section 11-B, North Tangent
Plan View of Test Area

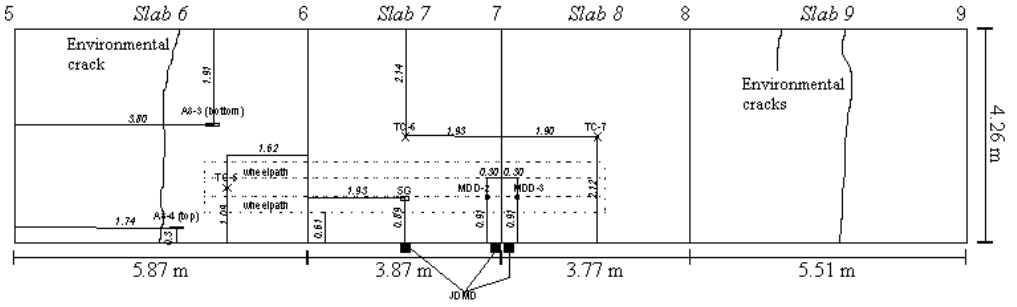

Section 11-C, North Tangent
Plan View of Test Area

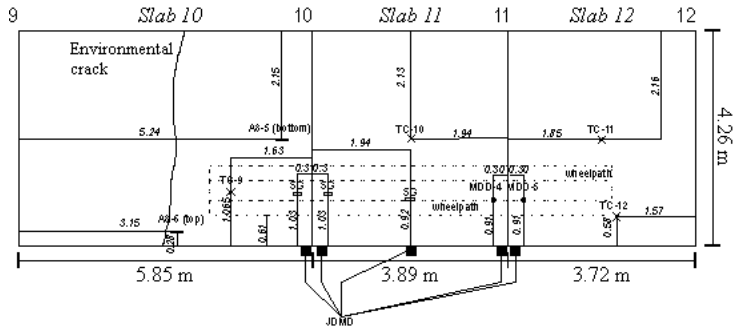

Section 11-D, North Tangent
Plan View of Test Area

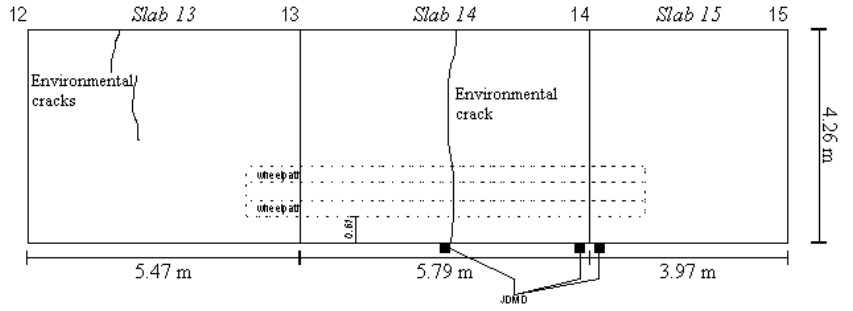

Section 9-D, North Tangent
Plan View of Test Area

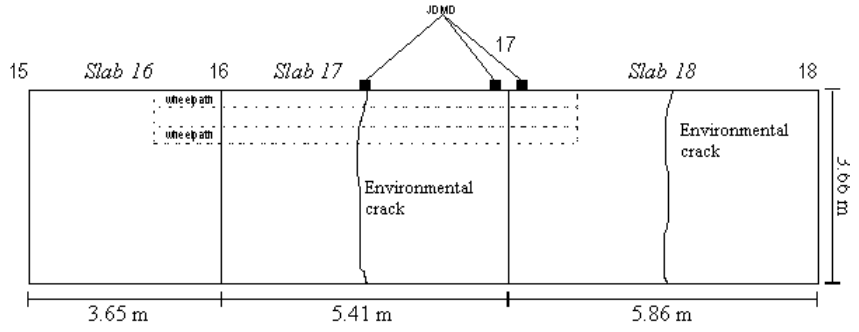

Section 9-B, North Tangent
Plan View of Test Area

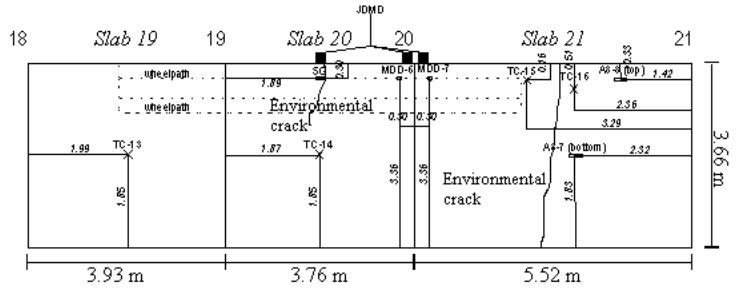

Section 9-C, North Tangent
Plan View of Test Area

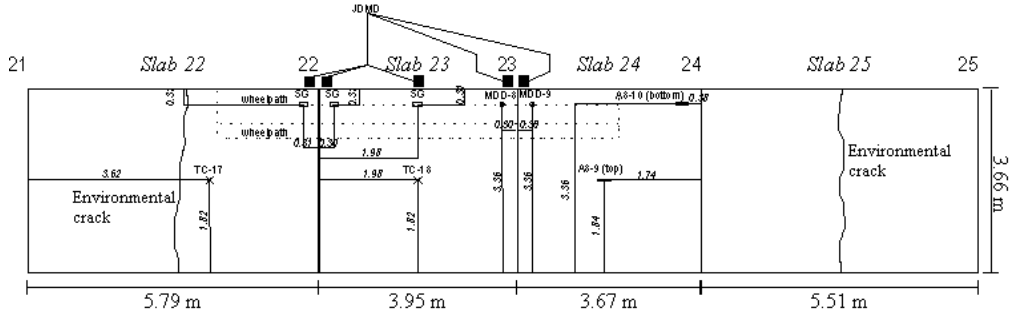

Section 9-A, North Tangent
Plan View of Test Area

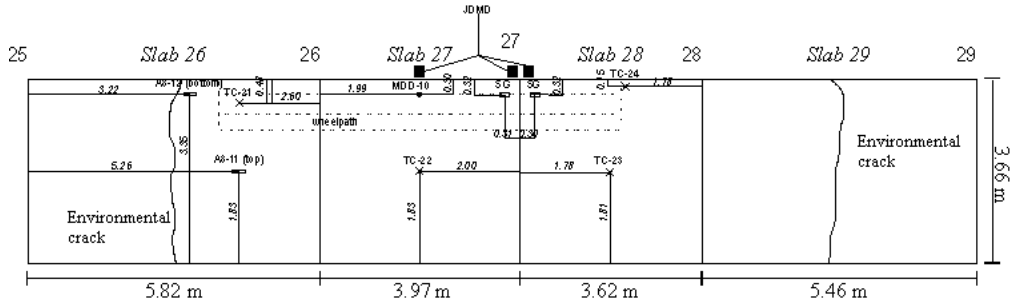

Section 7-A, North Tangent
Plan View of Test Area

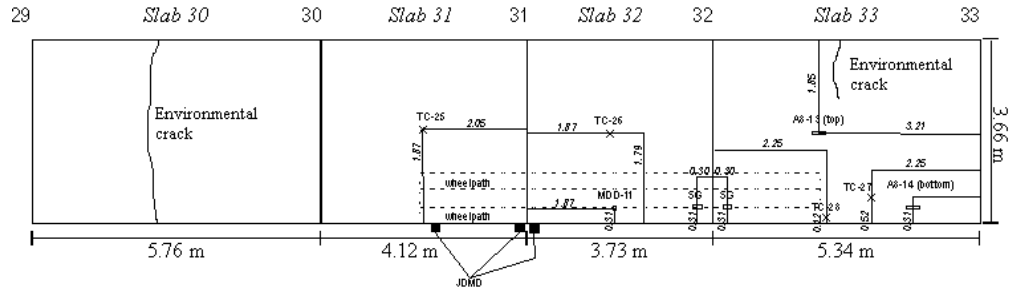

Section 7-B, North Tangent
Plan View of Test Area

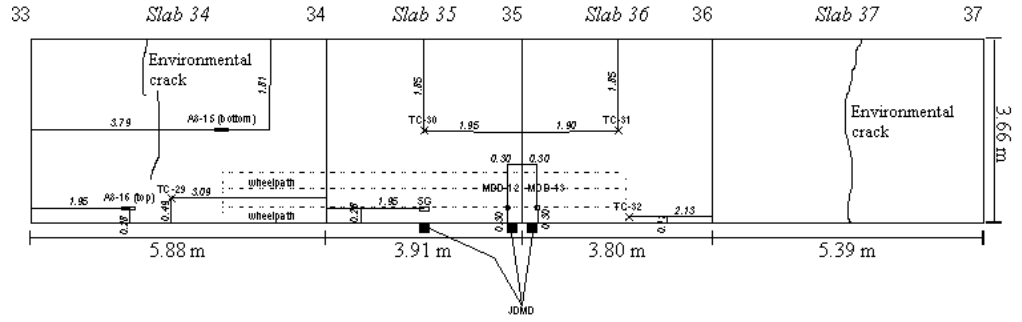

Section 7-C, North Tangent
Plan View of Test Area

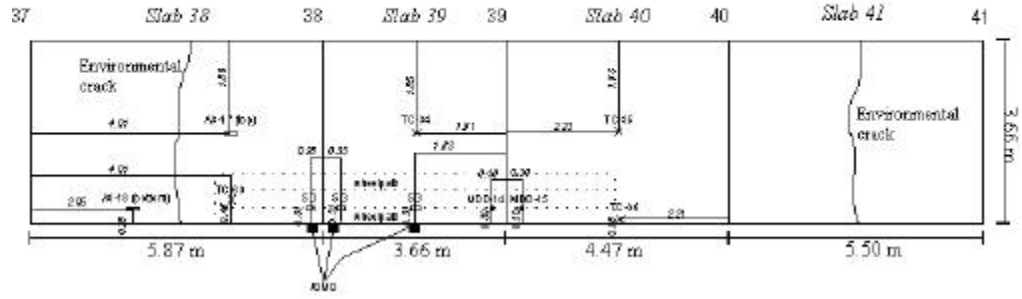

Section 7-D, North Tangent
Plan View of Test Area

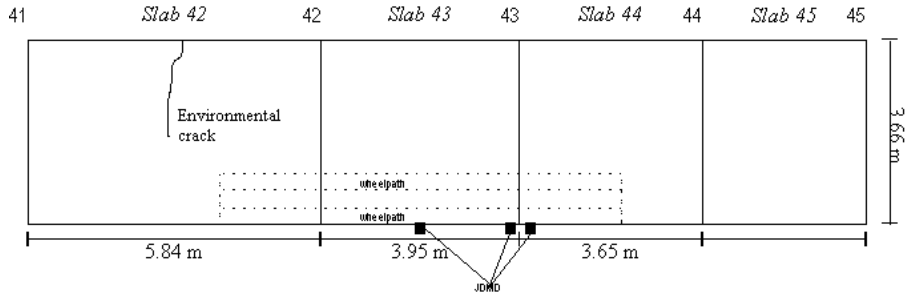

Section 1-A, South Tangent
Plan View of Test Area

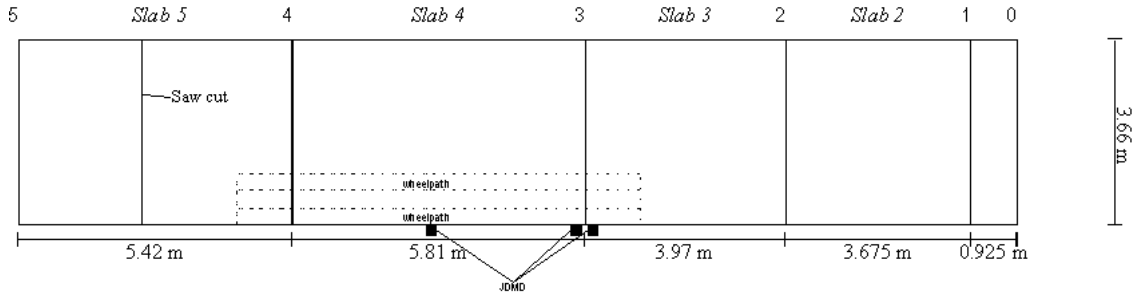

Section 1-B, South Tangent
Plan View of Test Area

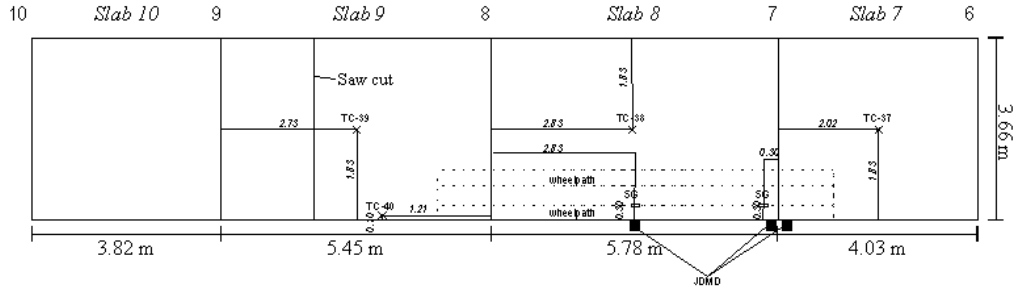

Section 1-C, South Tangent
Plan View of Test Area

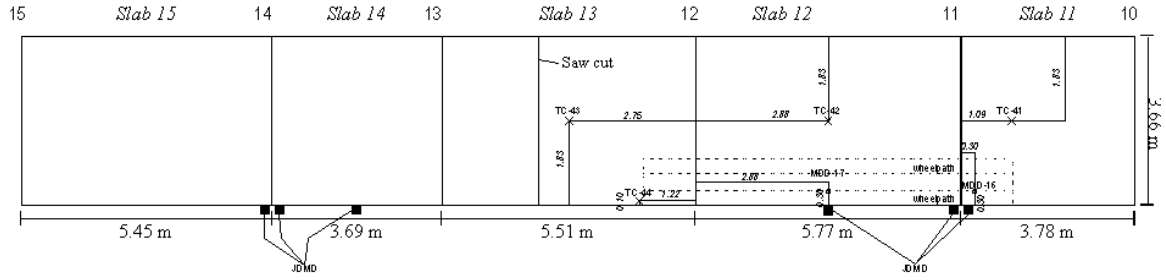

Section 3-A, South Tangent
Plan View of Test Area

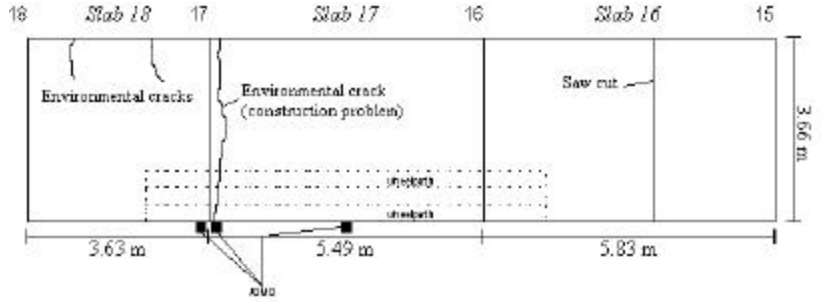

Section 3-B, South Tangent
Plan View of Test Area

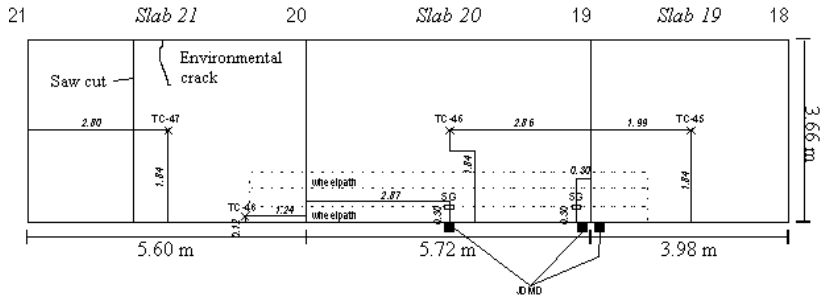

Section 3-C, South Tangent
Plan View of Test Area

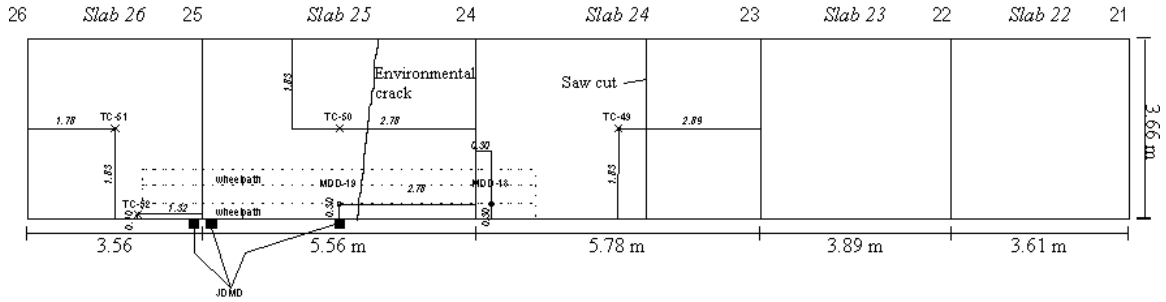

Section 3-D, South Tangent
Plan View of Test Area

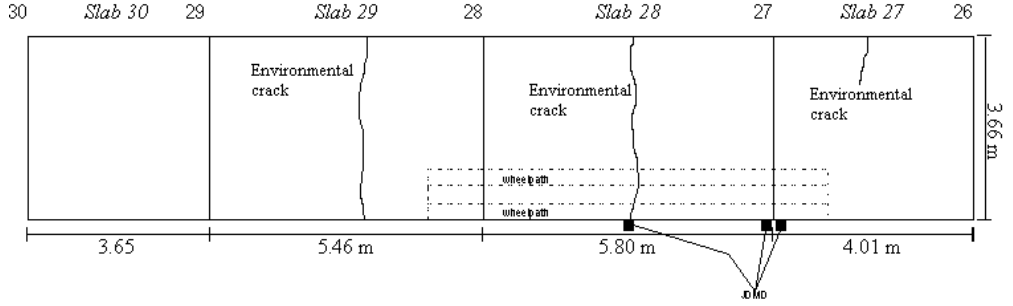

Section 5-A, South Tangent
Plan View of Test Area

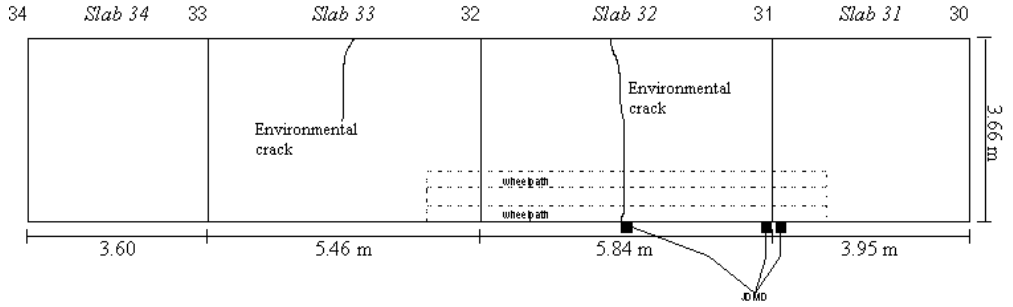

Section 5-B, South Tangent
Plan View of Test Area

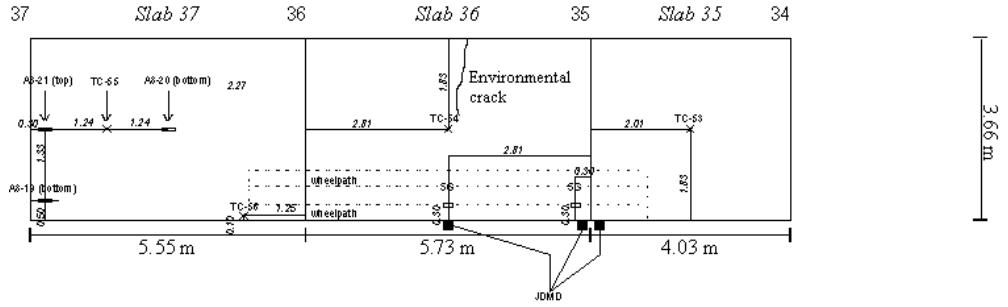

Section 5-C, South Tangent
Plan View of Test Area

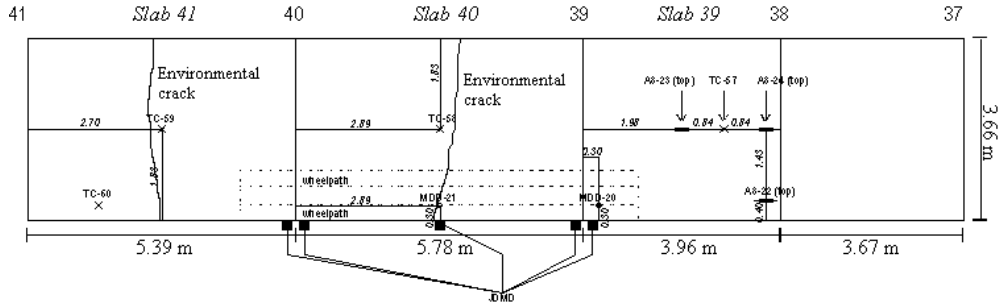

Section 5-D, South Tangent
Plan View of Test Area